ISTANBUL TECHNICAL UNIVERSITY ⋆ INSTITUTE OF SCIENCE AND TECHNOLOGY

DISPERSION AND WAVEGUIDING OF ULTRASLOW LIGHT IN ATOMIC BOSE-EINSTEIN CONDENSATES

Ph.D. Thesis by

Devrim TARHAN

Department : Physics

Programme : Physics Engineering

JANUARY 2007

ISTANBUL TECHNICAL UNIVERSITY ⋆ INSTITUTE OF SCIENCE AND TECHNOLOGY

DISPERSION AND WAVEGUIDING OF ULTRASLOW LIGHT IN ATOMIC BOSE-EINSTEIN CONDENSATES

Ph.D. Thesis by

Devrim TARHAN

(509022055)

Date of submission : 30 November 2006

Date of defence examination : 09 January 2007

Supervisor (Chairman) : Assoc. Prof. Dr. Nazmi POSTACIOĞLU

Cosupervisor : Assoc. Prof. Dr. Özgür MÜSTECAPLIOĞLU (KÜ)

Members of the Examining Committee Prof. Dr. Ömer F. DAYI (İTÜ)

Prof. Dr. Nurfer GÜNGÖR (İTÜ)

Prof. Dr. Ahmet Togo GİZ (İTÜ)

Prof. Dr. Alphan SENNAROĞLU (KÜ)

Prof. Dr. Nihat BERKER (KÜ)

JANUARY 2007

İSTANBUL TEKNİK ÜNİVERSİTESİ ⋆ FEN BİLİMLERİ ENSTİTÜSÜ

ATOMİK BOSE-EINSTEIN YOĞUŞUK MADDESİNDE ULTRA YAVAŞ IŞIĞIN DAĞINIMI VE DALGA KLAVUZLANMASI

DOKTORA TEZİ

Devrim TARHAN

(509022055)

Tezin Enstitüye Verildiği Tarih : 30 Kasım 2006

Tezin Savunulduğu Tarih : 09 Ocak 2007

Tez Danışmanı : Doç. Dr. Nazmi POSTACIOĞLU

Tez Eş Danışmanı : Doç. Dr. Özgür MÜSTECAPLIOĞLU (KOÜ)

Diger Jüri Üyeleri Prof. Dr. Ömer F. DAYI (İTÜ)

Prof. Dr. Nurfer GÜNGÖR (İTÜ)

Prof. Dr. Ahmet Togo GİZ (İTÜ)

Prof. Dr. Alphan SENNAROĞLU (KOÜ)

Prof. Dr. Nihat BERKER (KÜ)

OCAK 2007

DEDICATION

To my wife : I dedicate this work to my wife Nilgün. Nilgün has really given up a lot so that I could follow physics. She has been patient, supportive, and understanding when sometimes physics came first. I hope I can make it up to her.

ACKNOWLEDGEMENTS

I would like to thank to my supervisor Assoc. Prof. Dr. Nazmi POSTACIOĞLU and to my co-supervisor Asst. Prof. Dr. Özgür MÜSTECAPLIOĞLU for their supports, advices during the preparation of this thesis and for their guidance and continual encouragement throughout this work. I should also like to thank to Prof. Dr. Alphan SENNAROĞLU for many comments during the course of this work.

Additionally I would also like to thank to Seçkin Sefi for helping with numerical computing.

This thesis was supported by Istanbul Technical University Foundation (ITU BAP) under Project No. 31192 and was partially supported by TÜBA. I must also thank to my wife, Nilgün Tarhan and to my mother and father for their constant support.

JANUARY, 2007 Devrim Tarhan

CONTENT

ABBREVIATIONS **v**
LIST OF TABLES **vi**
LIST OF FIGURES **vii**
LIST OF SYMBOLS **xi**
SUMMARY **xii**
ÖZET **xiii**

1. INTRODUCTION **1**

2. BOSE-EINSTEIN CONDENSATION **7**
2.1. Bose gas in harmonic trap 7
2.2. Gross-Pitaevskii equation 9
2.3. Density profile of BEC 9

3. ELECTRIC SUSCEPTIBILITY **13**
3.1. Electromagnetically Induced Transparency 13
3.2. Refractive Index enhancement 17

4. LINEAR AND NONLINEAR WAVE PROPAGATION **19**
4.1. Wave equation in dispersive Media 19
4.2. Numerical scheme for ultraslow-light pulse propagation 21
4.3. Propagation and dispersion of ultraslow-light pulses 22
4.4. Light propagation and mode dispersion 25
4.5. Numerical scheme for optical waveguiding 26
4.6. Nonlinear wave propagation 27
4.7. Transmission with electromagnetically induced transparency 29

5. RESULTS AND DISCUSSION **30**
5.1. Dispersive effects on BEC 30
5.2. Ultraslow optical waveguiding in BEC 45
5.3. Optical waveguiding under refractive index enhancement scheme 48
5.3. Compensation of ultraslow short pulses by nonlinear term 50
5.3. Group-velocity dispersion and self-phase modulation 52

6. CONCLUSION **54**

REFERENCES **57**

BIOGRAPHY **61**

ABBREVIATIONS

BEC	:	Bose-Einstein Condensate
EIT	:	Electromagnetically Induced Transparency
GPE	:	Gross-Pitaevskii Equation
GVD	:	Group-velociy Dispersion
SPM	:	Self-phase Modulation

LIST OF TABLES

5.1 Propagation constants obtained by WKB method 50

5.2 Numerically evaluated propagation constants 50

LIST OF FIGURES

2.1 Density profile of the semi ideal BEC. Spatial density profile of ^{23}Na the semi ideal Bose-Einstein condensate of $N = 8.3 \times 10^6$ atoms at $T = 43$ nK. ρ is scaled by the peak density. Trap parameters are chosen to be $\omega_r = 2\pi \times 69$ Hz and $\omega_z = 2\pi \times 21$ Hz. 10

2.2 Axial density profile of the semi ideal BEC.Axial density profile of ^{23}Na the semi ideal Bose-Einstein condensate of $N = 8.3 \times 10^6$ atoms at $T = 43$ nK. ρ is scaled by the peak density. Trap parameters are chosen to be $\omega_r = 2\pi \times 69$ Hz and $\omega_z = 2\pi \times 21$ Hz. 11

3.1 Schematic energy level diagram for EIT. Schematic energy level diagram of a three-level atom interacting with two laser beams in Λ configuration. 15

3.2 Real part of the EIT susceptibility. Real part of the electromagnetically induced transparency susceptibility as a function of normalized detuning. 16

3.3 Imaginer part of the EIT susceptibility. Imaginer part of the electromagnetically induced transparency susceptibility as a function of normalized detuning. 17

3.4 Schematic energy level diagram of the upper-level microwave scheme. 17

3.5 Display of index of refraction. Index of refraction of the core is displayed for some numerical values such as $n_1 = \sqrt{1 + A} = 1.12$ and $n_2 = 1$. 18

5.1 Contour plot of the propagation of pulse width $\tau = 10^{-6}$s. Contour plot of the propagation of an EIT pulse of width $\tau = 10^{-6}$s through a ^{23}Na BEC is displayed and time and position are in dimensionless units as explained in the text. 31

5.2 Contour plot of the propagation of pulse width $\tau = 10^{-7}$s. Contour plot of the propagation of an EIT pulse of width $\tau = 10^{-7}$s through a ^{23}Na BEC is shown and time and position are in dimensionless units as explained in the text. 32

5.3 Axial density profile of BEC. Axial density profile of ^{23}Na the Bose-Einstein condensate of $N = 8.3 \times 10^6$ atoms at $T = 43$ nK. ρ is scaled by the peak density. Trap parameters are chosen to be $\omega_r = 2\pi \times 69$ Hz and $\omega_z = 2\pi \times 21$ Hz. 33

5.4 Spatial dependence of group velocity. Spatial dependence of the local group velocity of a resonant probe pulse along the z-axis, with $\Delta = 0$, propagating through a ^{23}Na the Bose-Einstein condensate of $N = 8.3 \times 10^6$ atoms at $T = 43$ nK under EIT scheme. The parameters used are $M = 23$ amu, $a_s = 2.75$ nm, $\lambda_0 = 589$ nm, $\gamma = 2\pi \times 10.01$ MHz, $\Gamma_3 = 0.5\gamma$, $\Omega_c = 0.56\gamma$, $\Gamma_2 = 2\pi \times 10^3$ Hz. . 34

5.5 The absorption coefficient. Position dependence of the absorption coefficient α along the z-axis is displayed. The parameters are the same with those of figure(5.4) 35

5.6 Second-order dispersion coefficient. Axial spatial profile of the second-order dispersion coefficient b_2 for the parameters same with those of figure(5.4). Vertical axis is scaled by the peak value of b_2 which is ~ 0.108 s$^2/nm$. 36

5.7 Thermal behavior of the ρ_0 and the effective axial length L. Thermal behavior of the peak ρ_0 and the effective axial length L of the atomic density distribution, given by the semi-ideal model are shown. The parameters are the same with those of figure(5.4). . . 38

5.8 Thermal behavior of the broadening of a nanosecond pulse obtained analytically by an effective dispersive zone treatment. The solid, dashed, dotted and dot-dashed lines are for $a_s = 2.75, 3.75, 5.75$ nm, and $a_s = 7$ nm, respectively. The other parameters are the same with those of figure(5.4) [51, 54]. 40

5.9 Thermal behavior of the broadening of a nanosecond pulse determined by numerical simulations. The solid and dashed lines are for $a_s = 2.75$ nm and $a_s = 7$ nm, respectively. The other parameters are the same with those of figure(5.4) [51, 54] 40

5.10 Propagation of a nanosecond pulse through the interacting BEC. Time (t) is scaled by $0.4\,\mu$s. and position (z) is by $10\,\mu$m. The parameters are the same with those of figure(5.4) [51, 54]. 41

5.11 Propagation of a pulse of width $0.1\,\mu$s through the interacting BEC. Time (t) is scaled by $0.4\,\mu$s. and position (z) is by $10\,\mu$m. The parameters are the same with those of figure(5.4). 43

5.12 Propagation of a microsecond pulse through the interacting BEC. Time (t) is scaled by $0.4\,\mu$s. and position (z) is by $10\,\mu$m. The parameters are the same with those of figure(5.4) [51, 54]. 43

5.13 Coherent optical information storage capacity C (dimensionless) as a function of coupling field Rabi frequency Ω_c, scaled by γ. Parameters used are $L = 100\,\mu$m, $\tau_0 = 1\,\mu$s (solid line), $\tau_0 = 0.1\,\mu$s (dashed line), $\tau_0 = 0.01\,\mu$s (dot-dashed line), $\rho = 10^{21}\,\mathrm{m}^{-3}$. The other parameters are the same with those of figure(5.4) [51, 54]. . 44

5.14 Dependence of the group velocity on $K = (l + 2m + 1)$ at $T = 42$ nK. For the single mode condition group velocity is 30.8 m/s [53, 55]. 46

5.15 Temperature dependence of V in EIT scheme. Parameters used are $a_s = 2.75$ nm, $\lambda = 589$ nm, $N = 8.3\times10^6$ ^{23}Na atoms, $\omega_r = 2\pi\times69$ Hz, $\omega_z = 2\pi \times 21$ Hz 47

5.16 Radial profiles of transverse modes LP_{00} and LP_{10} confined in a BEC of ^{23}Na atoms with parameters given in the figure 5.15. . . . 48

5.17 LP_{00}, LP_{01}, LP_{02}, LP_{03} are displayed. Each $\psi(r)$ is shown and the smallest root is solid line. 49

5.18 Temperature dependent of V in refractive index enhancement scheme. Parameters used are: Scattering length, $a_s = 2.75$nm, $\lambda = 589$nm, $N = 8.3 \times 10^6$, $\omega_r = 2\pi \times 69$Hz, $\omega_z = 2\pi \times 21$Hz, $M = 23$amu as for the experiment [1]. 49

5.19 Radial profiles of transverse modes LP_{00} and LP_{10} confined in a BEC of ^{23}Na atoms with parameters given in the figure 5.18. . . . 50

5.20 Axial spatial profile of the nonlinear coefficient γ for the parameters same with those of figure(5.4). γ is normalized by 1.437×10^{-3} . 51

5.21 Axial spatial profile of the second-order dispersion coefficient β_2 for the parameters same with those of figure(5.4). β_2 is normalized by 1.06×10^{-11} 52

LIST OF SYMBOLS

ρ	:	density
λ_{dB}	:	de-Broglie wave lenght
μ	:	Chemical potential
k_B	:	Boltzmann constant
T_c	:	Critical temperature of BEC
ω_r	:	Radial trap frequency
ω_z	:	Angular frequency in the z direction
a_s	:	Atomic s-wave scattering length
β_{lm}	:	Propagation constant in the z direction
q	:	Radial wave number
v_g	:	Group velocity
α	:	Loss term coefficient
b_2	:	Second-order dispersion coefficient
η	:	Nonlinear coefficient
λ	:	The wave length for ^{23}Na

DISPERSION AND WAVEGUIDING OF ULTRASLOW LIGHT IN ATOMIC BOSE-EINSTEIN CONDENSATES

SUMMARY

We investigate potential of atomic Bose-Einstein condensates as dynamic memory devices for coherent optical information processing. Specifically, the number of ultra-slow pulses that can be simultaneously present within the storage time in the condensate has been analyzed. By modelling short pulse propagation through the condensate, taking into account high-order dispersive properties, constraints on the information storage capacity has been discussed. The roles of temperature, spatial inhomogeneity, the interatomic interactions and the coupling laser on the pulse shape have been pointed out. For a restricted set of parameters, it has been found that coherent optical information storage capacity would be optimized. The conditions determining the number of optical modes that can be supported by an atomic Bose-Einstein condensate are also investigated. We investigate waveguiding of ultraslow light pulses in an atomic Bose-Einstein condensate. We show that under the conditions of off-resonant electromagnetically induced transparency, waveguiding with a few ultraslow modes can be realized. We show that under the conditions of refractive index enhancement via quantum coherence, it is possible to control the number of modes by means of experimentally accessible parameters including trap size, temperature, condensate number density and scattering lengths. Analytical results for the single and two-mode conditions are found. We show that under the conditions of off-resonant electromagnetically induced transparency, waveguiding with a few ultraslow modes can be realized. Results of numerical simulations are compared with analytical calculations of the propagation constants for a parabolic-refractive index profile. Moreover, we examine short pulse propagation through the atomic Bose-Einstein condensates taking into account Kerr nonlinearity and second-order dispersive effect. The roles of Kerr nonlinearity on the pulse shape have been examined on pulse width with 0.01μsec.

ATOMİK BOSE-EINSTEIN YOĞUŞUK MADDESİNDE ULTRA YAVAŞ IŞIĞIN DAĞINIMI VE DALGA KLAVUZLANMASI

ÖZET

Bose-Einstein yoğuşuk maddesini uyumlu optik bilgi işlemleri için dinamik hafıza aleti olarak araştırdık. Özellikle, yoğuşuk maddede depolama zamanı içinde çok yavaş optik darbeler analiz edildi. Yüksek dereceden dağınım özellikleri hesaba katarak yoğuşuk maddede optik darbelerin ilerlemesini modelledik. Bu çalışmada atomik sistemin konuma bağlı olarak değişen yoğunluğu, sıcaklık ve atomik çarpışmaların şiddetine göre değişen yoğunluk profili de dikkate alındı. Yapılan sayısal ve analitik hesaplar ile kısa darbenin genişlemesini sıcaklığa, konuma ve atomik çarpışmalara göre analiz ettik. Bir optik darbe yoğuşuk madde içinde rezonans frekansında elektromanyetik olarak indüklenmiş saydamlık etkisi ile çok yavaş ilerletilebilir. Sınırlı parametreler için eşevreli optik bilgi hafıza kapasitesi bulundu. Radyal yöndeki yoğunluk profilini dikkate alan ve fiber optikte eğimli indeks fiber profili ile yoğuşuk maddenin kırılma indisini modelledik. Ayrıca madde içinde çok yavaş optik darbeler gözlendi. Bu da rezonans olmayan elektromanyetik olarak indüklenmiş saydamlık koşulları altında gerçekleştirildi. Yoğunlaşmış maddenin taşıyabileceği mod sayısını hem analitik hem de sayısal olarak irdeledik. Ayrıca optik darbelerin Bose-Einstein yoğuşuk (BEY) maddesinde ilerlemesinde üç boyutlu etkiler ve optik modların sayısındaki bağ koşullar incelendi. Kırılma indisi arttırılması durumunda daha çok optik modun (BEY) maddesinde taşınabileceğini gösterdik. Mod sayısının sıcaklığa bağlı değişimini inceledik. Kuantum eşevrelik sayesinde, deneysel parametreleri kullanarak mod sayısının kontrol edilebileceğini gösterdik. Ayrıca tek ve çok mod koşulları analitik olarak bulundu. Analitik sonuçlar, sayısal sonuçlarla kontrol edildi. Ek olarak, kısa optik darbelerin Bose-Einstein yoğuşuk maddesinde ilerlemesinde ikinci dereceden dağınım etkisini ve nonlineer optik Kerr etkisini inceledik. Kerr nonlineer katsayısının darbe genişliği 0.01μsn olan darbe üzerinde etkisi incelendi.

1 INTRODUCTION

Laser pulses are widely used in today's communication systems due to their high speeds, stability and ease of transport. In modern communication technologies, it is an undoubtedly important, essential and high priority objective to transfer more information in a shorter time span. It is also important for internet with its ever growing number of users, wireless communication systems and satellite controlled guidance. For these reasons optical based computer is expected to be developed in the near future. In parallel, it is an indispensable condition that information encoded with optical pulses should be stored without deformation for a long time.

Short pulses, in comparison to longer ones, are more susceptible to the dispersive character of the medium, where they propagate or are stored. This demands new approaches in their theoretical modelling. This thesis aims to develop a general, detailed and realistic theory of pulse propagation that also takes into account high order dispersive and nonlinear properties of the medium carrying or storing short pulses, and using this theory in order to reveal most efficient and advantageous mediums and schemes for optical fast information transfer and storage.

Recently, optical memories has been developed via slowing down long optical pulses in atomic Bose-Einstein condensates, Ruby crystal, and Rb gas . By investigating interactions of such materials such as Bose-Einstein condensate with shorter pulses, the conditions to enhance their capacities are demonstrated. In the second part of the thesis, information transport from optical memory to fiber optics system has been explored. The aim of this thesis is to investigate the influence of the optical pulse on the medium of propagation or storage.The linear optics theory developed in the first part has been generalized to a theory taking into account non-linear effects, such as optical Kerr effect, and multi-photon absorption. Solutions to Electromagnetic Maxwell propagation equations coupled with

model Schrödinger equations for the material carrying or storing the light will be explored. By this way, quantum coherence stability of the medium has been understood at the atomic scale which is important for next generation informatics applications and quantum communication, quantum computation.

The remarkable achievement of ultraslow light[1, 2, 3] in a Bose-Einstein condensate (BEC), using electromagnetically induced transparency[4, 5] (EIT), inspired many intriguing and attractive applications[6, 7, 8, 9], in particular quantum optical dynamic memories[10, 11, 12, 13, 14]. Another way saying is since the first demonstration of ultra-slow light propagation through a Bose-Einstein condensate (BEC), a major application of slow light has been argued to be an optical memory. A key component of a quantum information processor would be the dynamic memory storage device. BECs have the potential to be used in such an application. Consider a sequence of information bits carried by a train of optical pulses. Upon injection into a BEC, the coherent optical information can be stored for a period given by the transit time of the pulses. In the BEC phase, the demonstrated ultra-slow group velocities allow for long storage periods of the order of few microseconds. Operational performance of such a device can be characterized by the overall bit storage capacity of the BEC, which can be defined as the number of optical pulses that can be simultaneously stored during the storage time in the BEC.

In order to make quantum memories more practical for quantum information processing, it is useful to enhance their bit storage capacity. This would be possible, in principle, by using pulses temporally as short as possible so that more pulses can be injected into the BEC during the storage time[15]. Early ultraslow light experiments use pulses of widths few microseconds. Shorter pulses would have longer frequency bandwidths, beyond the EIT window. EIT window can be modified by an external magnetic field[16]. Very recently, it has been experimentally demonstrated that EIT in a resonant atomic medium is possible for a comb of picosecond pulses[17]. Promising schemes to introduce large controllable time delays for such ultrashort pulses has been proposed where EIT window is overcome by using spatial and temporal processing[18]. Distortions in the shape of a large-bandwidth pulse have been experimentally studied in warm Rb vapor[19].

Shapes of the stored pulses will depend on the dispersive characteristics of the BEC. In particular, each pulse in the train will undergo dispersive broadening. The temporal separation of the pulses should be adjusted in such a way that after broadening in the BEC, consecutive pulses do not have significant spatial overlap. This sets the limit to the bit storage capacity of the BEC and can be estimated from the overall group delay and pulse broadening. It is therefore necessary to investigate the dispersive effects inside a BEC and develop accurate models that describe pulse propagation.

In this thesis, we consider propagation of short pulses with widths in the microseconds to nanoseconds range. In particular, we investigate the role of dispersion on the temporal characteristics of optical pulses propagating inside a BEC. Analytical formulas are first summarized for the constitutive relations from which the group delay, absorption coefficient, and the second-order group delay dispersion can be calculated. We find that third and higher-order dispersion effects are negligible. The influence of the spatial inhomogeneity of the BEC, the interatomic scattering interactions and the temperature on the pulse shape are taken into account in our treatment. We show that just below the critical temperature of condensation, broadening becomes maximum. Finally, we give analytical formulas for the bit storage capacity of a BEC and determine its optimum performance. Information storage capacity of such an optical memory based upon slowing laser pulses down to subluminal speeds in BECs would strongly depend on the temporal width of the pulses. As the temporal width of the pulses gets smaller, condensate could contain more pulses in a given time interval. Unfortunately, one cannot hope to use shortest pulses (such as femtosecond or even attosecond) available to maximize information capacity. A challenging issue to use such a short pulse in condensates is the fact that slow-light scheme in BEC is based upon electromagnetically induced transparency (EIT) which occurs for not so broad optical frequency window. On the other hand, temporally short pulses have large frequency widths. Present experimental set ups use optical pulses of temporal widths in the order of microseconds. We note that EIT conditions can be reasonably well satisfied for pulses of widths $\sim 10^{-7}$ which would enhance the information capacity of the condensate ten times more.

Another challenging issue in using short pulses in BECs is that their susceptibility to dispersion which may distort the pulse shape. We note that even though dispersive effects have been found small experimentally for microsecond pulses, there is no guarantee that role of dispersion would be small when we make the pulse ten times shorter. As the earlier theoretical models ignore the dispersion completely[35, 36], it is necessary to develop a more general theory of slow light propagation taking into account the higher order dispersive properties of the BEC. In the present paper we develop such a theory, generalizing theory of dispersive EIT in a thermal uniform gas. Using our general theory, we have found that dispersive effects are insignificant for microsecond pulses used in slow-light experiments. However, temporal width of microsecond is the critical width below which dispersion starts to distort the pulse shape. We show that at a width of 10^{-7} seconds, dispersion leads to a small temporal broadening of the pulse.

It may be noted here that study of dispersive effects in slow-short-light propagation may lead to alternative applications such as determination of condensate temperature through measurement of broadening, pulse shape engineering, and frequency band narrowing. While we treat the light classically, novel effects have been predicted for slow-light in quantum regime, in particular a new nonlinearity regime for quantum light. Our results may contribute to such studies as well. Furthermore, the theory in the present thesis can easily be extended to situations in which BEC can have an enhanced nonlinear optical response of BEC that might be utilized for dispersion compensation.

At temperatures below the critical temperature of Bose-Einstein condensation, spatial distribution of atoms in optical or magneto-optical traps can be described by a cigar-shaped ellipsoid profile. The ellipsoid consists of a central high-density region, where the condensed atoms lie, surrounded by a low-density thermal gas envelope. In a simple-minded picture, electric susceptibility of the Bose-Einstein condensate (BEC) would be proportional to its density. The refractive index of the central condensate part therefore can be slightly higher than that of the enveloping thermal gas. This situation is then analogous to the case of an optical fiber with a graded-index profile, in which the refractive-index of the central core decreases gradually from center to the core boundary. An important distinction from

the fibers is that atomic-condensates are resonant systems while the fibers are nonresonant optical propagation mediums. Exploiting quantum interference[4] in such atomic resonant medium, remarkable optical pulse propagation effects such as ultraslow light[1, 21, 22, 26, 36], superluminal light propagation[40, 41, 42, 43], stoppage[44] and storage[15] of optical pulses have been discovered. Most of the theoretical and experimental work has been restricted to one-dimensional situations. Dynamics of optical pulses in two or more dimensions has been investigated very recently numerically[45]. The possibility of changing the direction of the probe pulse via a control beam has been examined in detail. Other higher dimensional considerations have also been presented[35, 46]. Higher dimensional considerations may prove useful for quantum information processing and storing in addition to manipulation of classical optical pulses.

We investigate another effect of higher dimensional pulse propagation in a BEC, hinted by our analogy to optical fibers. The refractive index difference between the core and the cladding in a fiber influences the parameter which characterize the number of modes that can be supported by the fiber. In the case of BEC, condensate-thermal gas index difference is negligibly small unless close to an atomic resonance. In order to exploit the high density contrast between the condensate and the thermal gas to allow for multi-mode optical pulses, it is necessary to be close to an atomic resonance. Due to strong absorption nearby the atomic resonance, optical pulse could not propagate much in this case. In previous theoretical and experimental works, pulse propagation under the conditions of electromagnetically induced transparency (EIT) has been utilized to beat the absorption and manipulate the speed of light. However, in this case, the refractive index of the condensate remains almost the same with the thermal gas. Hence, under EIT conditions BEC acts as an essentially a single-mode medium. Strictly speaking it can support degenerate two polarization modes only. It has been theoretically shown that such polarization modes can be separated by detuning one of the components slightly away from the EIT resonance, at the cost of some absorption[47]. Light storage with light of arbitrary polarization has been demonstrated experimentally[48]. In order to support many modes while at the same time to beat absorption, we suggest to use a refractive index-enhancement scheme

as an alternative to EIT schemes considered so far.

The thesis is organized as follows.In chapter-2 we give a brief summary of the Bose-Einstein condensate. We discuss Bose gases in harmonic trap and give the definition of Gross-Pitaevskii equation. We have modelled density profile of the Bose-Einstein condensate . In chapter-3 we present the electric susceptibility of an interacting BEC under various atomic systems and electric susceptibility of an interacting BEC under EIT conditions and refractive index enhancement scheme is derived. In Chapter-4 we investigate the linear and nonlinear wave propagation. Wave equation in dispersive media for the EIT medium is derived. Propagation and dispersion of slow light under EIT scheme is discussed. Moreover we examine light propagation and mode dispersion in BEC. Furthermore nonlinear wave propagation in the medium is extensively examined. Chapter-5 contains results and discussion. We present and discuss our numerical and analytical results in Chapter-5. Finally, we conclude in the last chapter. This thesis provides useful model for the pulse propagation which will be used in quantum memory, optical data storage and quantum information and communication.

2 BOSE-EINSTEIN CONDENSATION

Experimental realization of Bose-Einstein condensation(BEC) in alkali atomic gases was achieved in 1995 for rubidium[24],sodium[25]. BEC occurs at low temperatures(μK to nK range). Bosons start to attract each other by bosonic stimulaton and form a macroscobic population in the ground state of the system. Another way of saying is, Bose-Condensation is formed when a macroscopic population of bosons occupy the same quantum state at non-zero temperature. Only when the atomic wave functions overlap and when there is significant probability to exist in the same state does the Bosonic symmetry become important. This brings about the temperature and density requirements for condensation. The small enhancement factor also grows as the number of atoms in the ground state becomes larger. BEC is matter-wave which is formed when atomic matter waves begin to overlap. The atomic wave start to overlap when the spacing between atoms, $d = \rho^{-1/3}$, becomes equal to their de-Broglie wavelength, $\lambda_{dB} = \sqrt{h/2\pi m k_B T}$. In other words, phase space density, $\rho\lambda_{bB}^3$ is the order of unity. The mass of the atom is defined as m, T is the temperature of the system. There are many reasons why we choose BEC as a material. One of the most important thing is, coherent matter waves which enable us to apply many intriguing and attractive applications in quantum optics. For example, the speed of light was reduced to $1 - 20$(m/sec) using BEC.[1]. Quantum coherence, quantum memory, non-linear wave mixing and quantum entanglement have been realized after the experimentally realization of the Bose-Einstein condensation(BEC).

2.1 Bose gases in a harmonic trap

The mean occupation number of the single-particle state ω is given by the Bose distribution function which is defined as [60],

$$f^0(\epsilon_\omega) = \frac{1}{e^{\beta(\epsilon_\omega - \mu)} - 1} \tag{2.1.1}$$

where $\beta = \frac{1}{k_B T}$ and ϵ_ω denotes the energy of the single-particle state for the particular trapping potential. Let us consider anisotropic harmonic oscillator potential, which is written as

$$V(r) = \frac{1}{2} m(\omega_x^2 x^2 + \omega_y^2 y^2 + \omega_z^2 z^2). \tag{2.1.2}$$

The energy levels, $\epsilon(n_x, n_y, n_z)$ are

$$\epsilon(n_x, n_y, n_z) = (n_x + \frac{1}{2})\hbar\omega_x + (n_y + \frac{1}{2})\hbar\omega_y + (n_z + \frac{1}{2})\hbar\omega_z. \tag{2.1.3}$$

where the numbers n_i assume all integer values greater than or equal to zero. If we determine the number states $G(\epsilon)$ with energy less than a given value ϵ, we will obtain[60]

$$G(\epsilon) = \frac{1}{6} \frac{\epsilon^3}{\hbar^3 \omega_x \omega_y \omega_z}. \tag{2.1.4}$$

Density of states, which is defined as $g(\epsilon) = \frac{\mathrm{dG}}{\mathrm{d}\epsilon}$ is given by[60]

$$g(\epsilon) = \frac{1}{2\hbar^3} \frac{\epsilon^2}{\omega_x \omega_y \omega_z} = C\varepsilon^2. \tag{2.1.5}$$

In equation (2.1.5) C is defined as $\frac{1}{2\hbar^3} \frac{1}{\omega_x \omega_y \omega_z}$. The number of particles in excited states is given by

$$N_{ex} = \int_0^\infty d\epsilon \, g(\epsilon) f^{\,0}(\epsilon). \tag{2.1.6}$$

At critical temperature, T_c chemical potential μ is equal to zero and total number of particles can be denoted as[60]

$$N = N_{ex}(T_c, \mu = 0) = \int_0^\infty d\epsilon \, g(\epsilon) \frac{1}{e^{\beta\epsilon_\omega} - 1}. \tag{2.1.7}$$

Equation (2.1.7) can be written by the dimensionless variable in terms of, $x = \epsilon / k_B T_c$

$$N = \frac{1}{2\hbar^3} \frac{\epsilon^2}{\omega_x \omega_y \omega_z} (k_B T_c)^3 \Gamma(3) \zeta(3). \tag{2.1.8}$$

where $\Gamma(3)$ is the gamma function and $\zeta(3)$ is the Riemann zeta function[60]. If we calculate critical temperature for three dimension anisotropic harmonic potential, we will obtain[60]

$$k_B T_c = \frac{\hbar \bar{\omega} N^{1/3}}{\zeta(3)^{1/3}} \approx 0.94 \hbar \bar{\omega} N^{1/3}. \tag{2.1.9}$$

Here $\bar{\omega}$ is the geometric average for harmonic potential which is defined as $\bar{\omega} = (\omega_x \omega_y \omega_z)^{1/3}$. One can find condensate fraction below the critical temperature by

equation (2.1.6). Below the critical temperature the number $N_e x$ of particles is given by $N_{ex} = C\Gamma(3)\zeta(3)(k_B T)^3$ and we can write it in the form

$$N_{ex} = N(\frac{T}{T_c})^3. \tag{2.1.10}$$

The number of particles in the condensate is $N_0(T) = N - N_{ex}(T)$. As a result for the three-dimensional harmonic oscillator potential condensate fraction can be denoted as[60]

$$\frac{N_0}{N} = [1 - (\frac{T}{T_c})^3]. \tag{2.1.11}$$

2.2 Gross-Pitaevskii equation

The condensate part of the Bose gas can be described by a macroscopic wave function, $\psi(\vec{r})$, which satisfies the Gross-Pitaevskii equation or nonlinear Schrödinger equation [60].

$$-\frac{\hbar^2}{2m}\nabla^2\psi(\vec{r}) + V(r)\psi(\overrightarrow{r}) + U_0|\psi|^2\psi(\vec{r}) = \mu\psi(\vec{r}). \tag{2.2.12}$$

where $U_0 = 4\pi\hbar^2 a_s/m$; m is atomic mass; a_s is the atomic s-wave scattering length,which determines the sign and the strength of interaction; μ is the chemical potential. For sodium, the scattering length is positive. The effect of kinetic energy, $-\frac{\hbar^2}{2m}\nabla^2\psi(\vec{r})$ is small for the experimental conditions, therefore we can neglect this term. The density profile of the condensate is approximately determined by the "Thomas-Fermi" approximation.

$$\rho(\vec{r}) = |\psi|^2 = \frac{1}{U_0}[\mu - V(\vec{r})]. \tag{2.2.13}$$

2.3 Density profile of BEC

At low temperatures a Bose gas can be considered to be composed of two components. The first component becomes the condensate part and the other is a thermal gas background. In a harmonic trap, spatial overlap between the components becomes small, which makes effects of collective elementary excitations weaker relative to those in homogeneous gases. This allows for semiclassical descriptions of density distributions in terms of the self-consistent Hartree-Fock model, which simplifies more general Hartree-Fock-Popov description[28]. When the thermal

component is dilute enough, one may further neglect the atomic interactions in the thermal component. Taking into account mean field repulsion only among the condensed atoms, an analytical explicit description of a partly condensed gas was developed and denoted as the semi-ideal model[29]. We will now briefly review this model, where condensate density is evaluated under Thomas-Fermi approximation[30, 31] to Gross-Pitaevskii equation[32, 33], and the thermal gas density is calculated semi-classically[34, 29]. The total density at a temperature T is then written to be

$$\rho(\vec{r}) = \frac{\mu - V(\vec{r})}{U_0}\Theta(\mu - V(\vec{r}))\Theta(T_C - T) + \frac{g_{3/2}(ze^{-\beta V})}{\lambda_T^3}, \tag{2.3.14}$$

where $U_0 = 4\pi\hbar^2 a_s/m$; m is atomic mass; a_s is the atomic s-wave scattering length; μ is the chemical potential; $\Theta(.)$ is the Heaviside step function; $g_n(x) = \Sigma_j\, x^j/j^n$ is the Bose function; λ_T is the thermal de Bröglie wavelength; $\beta = 1/k_B T$; $z = \exp(\beta\mu)$ is the fugacity, and T_C is the critical temperature. The external trapping potential is $V(\vec{r}) = (m/2)(\omega_r^2 r^2 + \omega_z^2 z^2)$ with ω_r the radial trap frequency and ω_z the angular frequency in the z direction. Spatial density profile of the Bose-Einstein condensate and axial density profile(1-dimension) of the BEC are shown in Figure (2.1) and Figure(2.2).

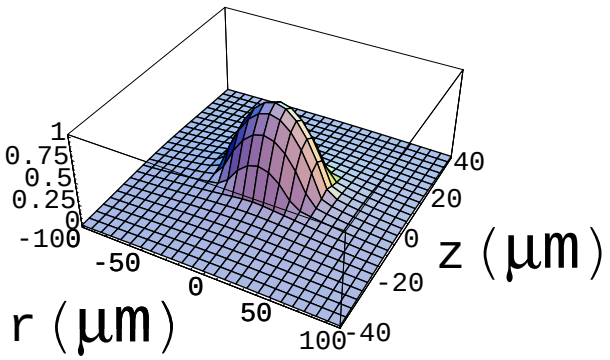


Figure 2.1: Density profile of the semi ideal BEC. Spatial density profile of ^{23}Na the semi ideal Bose-Einstein condensate of $N = 8.3 \times 10^6$ atoms at $T = 43$ nK. ρ is scaled by the peak density. Trap parameters are chosen to be $\omega_r = 2\pi \times 69$ Hz and $\omega_z = 2\pi \times 21$ Hz.

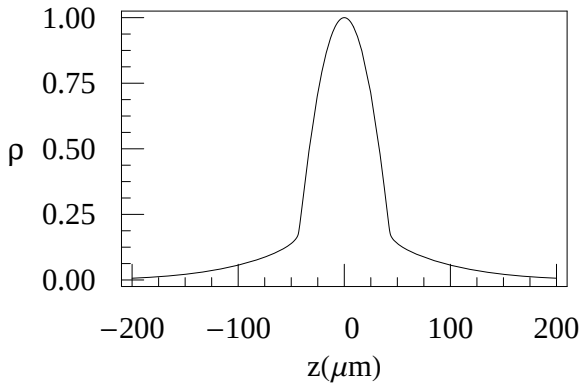


Figure 2.2: Axial density profile of the semi ideal BEC.Axial density profile of ^{23}Na the semi ideal Bose-Einstein condensate of $N = 8.3 \times 10^6$ atoms at $T = 43$ nK. ρ is scaled by the peak density. Trap parameters are chosen to be $\omega_r = 2\pi \times 69$ Hz and $\omega_z = 2\pi \times 21$ Hz.

μ is determined from $N = \int \mathrm{d}^3\vec{r}\rho(\vec{r})$. At temperatures below T_c this yields[29]

$$\mu = \mu_{TF}\left(\frac{N_0}{N}\right)^{2/5}, \tag{2.3.15}$$

where μ_{TF} is the chemical potential evaluated under Thomas-Fermi approximation and the condensate fraction is given by

$$\frac{N_0}{N} = 1 - x^3 - s\frac{\zeta(2)}{\zeta(3)}x^2(1-x^3)^{2/5}, \tag{2.3.16}$$

with $x = T/T_c$, and ζ is the Riemann-Zeta function. The scaling parameter s, characterizing the strength of atomic interactions within the condensate, is calculated to be[29, 28]

$$s = \frac{\mu_{TF}}{k_B T_C} = \frac{1}{2}\zeta(3)^{1/3}\left(15N^{1/6}\frac{a_s}{a_h}\right)^{2/5}. \tag{2.3.17}$$

Here, $a_h = \sqrt{\hbar/m(\omega_z\omega_r^2)^{1/3}}$ denotes the average harmonic oscillator length scale. At temperatures above the T_C, μ can be determined from $\mathrm{Li}_3(z) = \zeta(3)/x^3$, where $Li_3(.)$ is the third-order polylogarithm function. The semi-ideal model has a wide-range of validity in representing density distribution of a trapped Bose gas at finite temperature provided that $s < 0.4$[29]. At the same time the interactions are assumed to be strong enough to ensure $\mu \gg \hbar\omega_{r,z}$ so that kinetic energy of the condensate can be neglected according to the Thomas-Fermi approximation. In typical slow-light experiments in cold atomic gases, s remains within these limits. We shall use the semi-ideal model given density profile ρ in our investigations of

propagation and dispersion of slow pulses and present our explicit results in the next section.

3 ELECTRIC SUSCEPTIBILITY

The optical properties of atomic and molecular gases are fundementally tied to their intrinsic enery-level structure. The linear response of an atom to resonant light is described by the first-order susceptibility $\chi^{(1)}$. The imaginary part of this susceptibility $Im[\chi^{(1)}]$ determines the absorption, while the real part $Re[\chi^{(1)}]$ determines the refractive index [7]. One can calculate susceptibility via local density approximation. We determine the electric susceptibility χ of BEC consisting of such three-level atoms in EIT scheme and refractive index enhancement scheme. If we obtain electric susceptibility $\chi^{(1)}$ of an single atom, we can find the susceptibility of the system;

$$\chi \approx \rho(r)\chi^{(1)}. \tag{3.0.1}$$

3.1 Electromagnetically induced transparency

EIT is a technique for making cancellation of induced absorption to weak probe field tuned in resonance to an atomic transition by applying a strong resonant electromagnetic field to couple coherently another atomic transition[4]. Under EIT refractively thick gaseous medium becomes transparent to the probe beam. In order to formulate the effect, we consider a three-level atom, where the atomic states are denoted by $|1\rangle$, $|2\rangle$ and $|3\rangle$, Λ-type atom interacting with two lasers. Interaction of electromagnetic field with such an atom, under electric dipole approximation, can be described by a Hamiltonian of the form $H = H_0 + H_1$, where

$$\begin{aligned} H_0 &= \hbar\omega_1|1><1| + \hbar\omega_2|2><2| + \hbar\omega_3|3><3|, \\ H_1 &= -e\,\vec{r}\cdot\vec{E}(t). \end{aligned} \tag{3.1.2}$$

Here, H_0 and H_1 are unperturbed and interaction parts of the Hamiltonian, respectively. Probe laser, with angular frequency ω_p, is tuned to transition $|1>$ to $|3>$ while coupling laser, with angular frequency ω_c, is tuned to transition $|2>$ to $|3>$. We have assumed that only $|3> \rightarrow |1>$ and $|3> \rightarrow |2>$ transitions

are dipole allowed. The interaction part of the hamiltonian for the (EIT) system can be calculated by evaluating

$$H_1 = -(|1\rangle\langle 1| + |2\rangle\langle 2| + |3\rangle\langle 3|)e\,\vec{r}\cdot\vec{E}(t)(|1\rangle\langle 1| + |2\rangle\langle 2| + |3\rangle\langle 3|). \quad (3.1.3)$$

Denoting dipole matrix elements $\mu_{31} = \mu_{13}^* = e\langle 3|r|1\rangle$, $\mu_{32} = \mu_{23}^* = e\langle 3|r|2\rangle$, $\mu_{12} = \mu_{21}^* = e\langle 1|r|2\rangle$ and introducing slowly varying amplitudes for the electric fields $E_p(t) = (\varepsilon_p/2)\exp(-i\omega t)$ and $E_c(t) = (\varepsilon_c/2)\exp(-i\omega_c t)$, Rabi frequency for the coupling laser can be written as $\Omega_c = \mu_{32}\,\varepsilon_c/\hbar$. Interaction part of the hamiltonian becomes

$$\begin{aligned} H_1 &= -\frac{\hbar}{2}\{\frac{\mu_{31}\,\varepsilon}{\hbar}\exp(-i\omega t)|3\rangle\langle 1| \\ &+ \frac{\mu_{13}\,\varepsilon}{\hbar}\exp(i\omega t)|1\rangle\langle 3| \\ &+ \Omega_c\exp(-i\omega_c t)|3\rangle\langle 2| + \Omega_c\exp(i\omega_c t)|2\rangle\langle 3|\} \end{aligned} \quad (3.1.4)$$

Including the decay terms phenomenologically, to take into account the finite life time of the atomic levels, to the Liouville Equation $i\hbar\dot{\rho} = [H, \rho]$, density matrix equation become[56]

$$\dot{\rho} = -\frac{i}{\hbar}[H, \rho] - \frac{1}{2}\{\Gamma, \rho\} \quad (3.1.5)$$

where Γ is the relaxation matrix,which is defined by the equation $< n\,|\,\Gamma\,|\,m >= \gamma_n\,\delta_{nm}$. At the same time the relation between Γ and ρ is given by $\{\Gamma, \rho\} = \Gamma\rho + \rho\Gamma$. In terms of the matrix elements, explicit equation is given by (3.1.5) [56]

$$\dot{\rho_{\rm ij}} = -\frac{i}{\hbar}\sum_{\rm k}(H_{\rm ik}\rho_{\rm kj} - \rho_{\rm ik}H_{\rm kj}) - \frac{1}{2}\sum_{\rm k}(\Gamma_{\rm ik}\rho_{\rm kj} + \rho_{\rm ik}\Gamma_{\rm kj}). \quad (3.1.6)$$

The equation of motion for the density matrix elements ρ_{31} and ρ_{21} are given by

$$\begin{aligned} \dot{\rho_{31}} &= -(i\omega_{31} + \frac{\Gamma_3}{2})\rho_{31} \\ &- \frac{i}{2}\frac{\mu_{31}\varepsilon}{\hbar}\exp(-i\omega t)(\rho_{33} - \rho_{11}) + \frac{i}{2}\Omega_c\exp(-i\omega_c t)\rho_{21} \end{aligned} \quad (3.1.7)$$

$$\begin{aligned} \dot{\rho_{21}} &= -(i\omega_{21} + \frac{\Gamma_2}{2})\rho_{21} \\ &- \frac{i}{2}\frac{\mu_{31}\varepsilon}{\hbar}\exp(-i\omega t)\rho_{23} + \frac{i}{2}\Omega_c\exp(i\omega_c t)\rho_{31} \end{aligned} \quad (3.1.8)$$

The levels $|3> \rightarrow |1>$ are coupled by a probe field of amplitude ε and frequency ω , whose dispersion and absorption we are interested in. The dispersion and

absorption can be computed by ρ_{31}. All atoms are initially in the ground level $|1>$, $\rho_{11}^{(0)} = 1, \rho_{22}^{(0)} = \rho_{33}^{(0)} = \rho_{31}^{(0)} = 0$. In order to solve equation (3.1.7), we can write the equations in the matrix form [56],$\dot{R} = -MR + A$. where R, M and A are matrix elements. As a result R is given by $R = M^{-1}A$.

We found for the density matrix element ρ_{31},

$$\rho_{31} = \frac{i\mu_{31}\varepsilon \exp(-i\omega t)(i\Delta + \Gamma_2/2)}{2\hbar[(\Gamma_2/2 + i\Delta)(\Gamma_3/2 + i\Delta) + \frac{\Omega_c^2}{4}]} \tag{3.1.9}$$

Finally, we determine the electric susceptibility χ of BEC consisting of such three-level atoms in EIT scheme. If we use the relationship between electric field, atomic polarizability and (macroscopic) polarization[56], we find

$$\chi = \frac{\rho|\mu_{31}|^2}{\epsilon_0\hbar} \frac{i(i\Delta + \Gamma_2/2)}{[(\Gamma_2/2 + i\Delta)(\Gamma_3/2 + i\Delta) + \frac{\Omega_c^2}{4}]}, \tag{3.1.10}$$

where $\rho = \rho(\vec{r})$ stands for the inhomogeneous concentration of atoms in an interacting BEC. We consider a gas of N three-level atoms interacting with two laser beams in Λ configuration as shown in Figure3.1. In this scheme, it is assumed

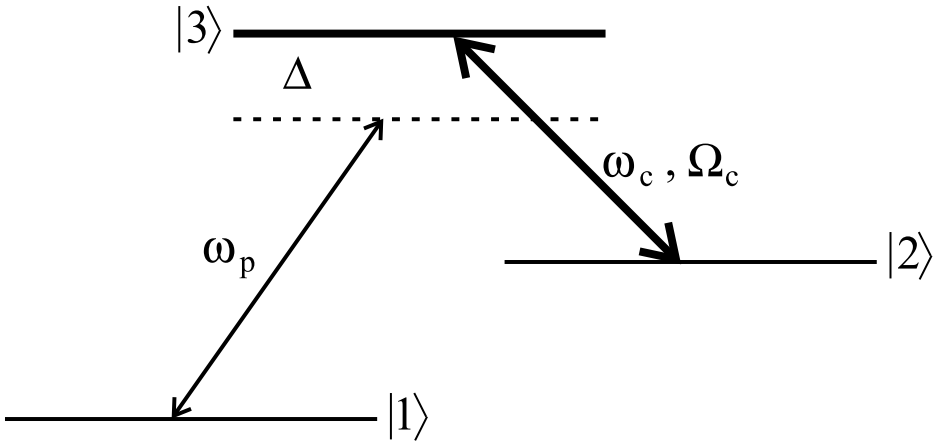


Figure 3.1: Schematic energy level diagram for EIT. Schematic energy level diagram of a three-level atom interacting with two laser beams in Λ configuration.

that the only dipole forbidden transition is the one between the lower levels. The upper level is coupled to the lower levels via a strong drive field with frequency ω_c and a weak probe field of frequency ω_p. This particular arrangement leads to the well-known effect of electromagnetically induced transparency (EIT) in which the absorption of the probe field at resonance is cancelled. The underlying physical mechanism of EIT is the quantum interference induced by the drive field.

Quantum coherence established between the lower level doublet put them in a dark state where excitations to the upper level become impossible. The transition probabilities destructively interfere for the two possible excitation routes to the upper level. In addition to turning an optically thick, opaque, medium transparent, EIT has recently been used for achieving ultra-slow light velocities, owing to the steep dispersion of the EIT susceptibility near the probe resonance. Susceptibility χ for the probe transition can be calculated as a linear response as most of the atoms remain in the lowest state. Assuming local density approximation, neglecting local field, multiple scattering and quantum corrections and employing steady state analysis, χ was found to be same as in Equation(3.1.11)[56]

$$\chi = \frac{\rho|\mu_{31}|^2}{\epsilon_0\hbar}\frac{i(i\Delta + \Gamma_2/2)}{[(\Gamma_2/2 + i\Delta)(\Gamma_3/2 + i\Delta) + \Omega_c^2/4]}, \tag{3.1.11}$$

where $\Delta = \omega_{31} - \omega_p$ is the frequency detuning of the probe field with frequency ω_p from the resonant electronic transition ω_{31}. For the cold gases considered in this paper and assuming co-propagating laser beams, Doppler shift in the detuning is neglected. Real and imaginer part of the EIT susceptibility is shown in the figures 3.2 and 3.3 respectively. It is assumed that the drive field is at resonance. Ω_c is the Rabi frequency of the drive field; μ_{31} is the dipole matrix element between states $|3\rangle$ and $|1\rangle$ which can also be expressed in terms of resonant wavelength λ_{31} of the probe transition via $\mu_{31}^2 = 3\epsilon_0\hbar\lambda_{31}^3\gamma/8\pi^2$ with γ is the radiation decay rate between $|3\rangle$ and $|1\rangle$. Γ_2 and Γ_3 denote the dephasing rates of the atomic coherences between the appropriate states. ρ stands for a given atomic density.

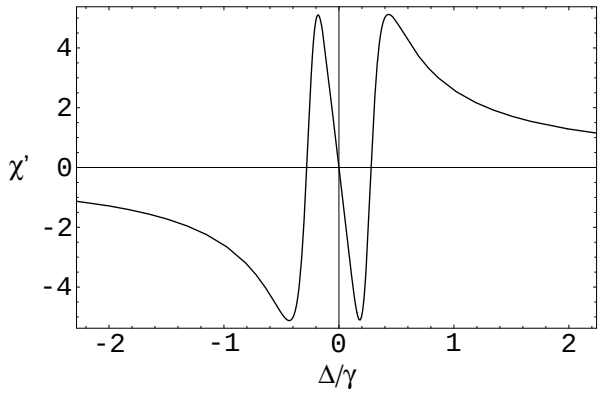


Figure 3.2: Real part of the EIT susceptibility. Real part of the electromagnetically induced transparency susceptibility as a function of normalized detuning.

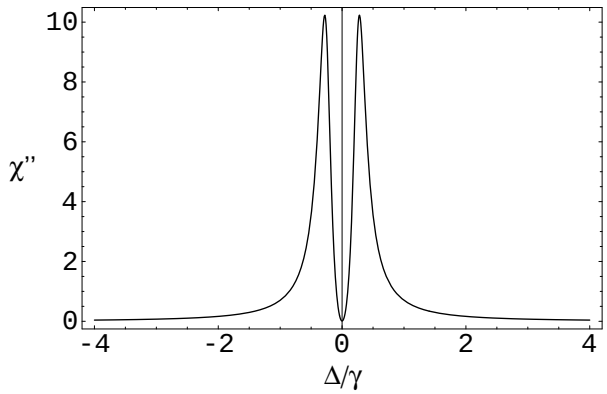


Figure 3.3: Imaginer part of the EIT susceptibility. Imaginer part of the electromagnetically induced transparency susceptibility as a function of normalized detuning.

3.2 Refractive index enhancement scheme

We now consider interaction of this condensate with external fields in a scheme designed for refractive-index enhancement by inducing quantum coherence. Specifically, we assume upper-level microwave scheme has been employed where the atomic level configuration is shown Figure(3.4). The excited level $|3\rangle$ is coupled

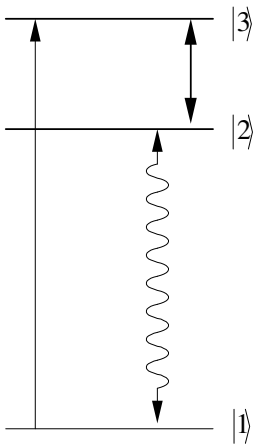


Figure 3.4: Schematic energy level diagram of the upper-level microwave scheme.

to the lower level $|2\rangle$ via a strong microwave field establishing the quantum coherence. Dipole transition between $|2\rangle$ and $|1\rangle$ is allowed. A pump mechanism from level $|1\rangle$ to $|3\rangle$ ensures an ultra high refractive index by maintaining a small fraction of atoms in level $|3\rangle$. By vanishing absorption, susceptibility (χ), becomes

a real number and can estimated to be [56]

$$\chi = \frac{3\lambda^2}{40\pi^2}\rho(r). \tag{3.2.12}$$

Here λ is the wavelength of $|2\rangle$ and $|1\rangle$ transition. For ^{23}Na gas, the wavelength λ, is $589nm$ and without local field correction susceptibility χ is 1.55. In our modelling of the refractive index, we shall specifically consider a gas of $N = 8.3 \times 10^6$ ^{23}Na atoms for which $M = 23$ amu, $\lambda = 589$ nm, $\gamma = 2\pi \times 10.01$MHz, $\Gamma_3 = 0.5\gamma$, $\Gamma_2 = 2\pi \times 10^3$ Hz, and $a_s = 2.75$ nm. For the parameters of the trapping potential, we take $\omega_r = 2\pi \times 69$ Hz and $\omega_z = 2\pi \times 21$ Hz as in reference [1]. Critical temperature for Bose-Einstein condensation for such a gas is found to be $T_C = 424$ nK. We calculate the refractive index by the formula $n = \sqrt{1+\chi}$. If we write the susceptibility again, we will obtain where R_{TF} is the Thomas-Fermi radius which is defined as $\sqrt{2\mu(T)/m\omega_r^2}$. Here A depends on susceptibility of the atomic systems. We denote the refractive index, $n(r)$ as

$$\chi(r) = \begin{cases} A[\{[1-(\frac{r}{R_{TF}})^2] & r \leq R_{TF} \\ 0 & r \geq R_{TF} \end{cases} \tag{3.2.13}$$

$$n(r) = \begin{cases} n_1[1-2\triangle(\frac{r}{R_{TF}})^2]^{1/2} & r \leq R_{TF} \\ n_1(1-2\Delta)^{1/2} & r \geq R_{TF} \end{cases} \tag{3.2.14}$$

where $2\triangle = (n_1^2 - n_2^2)/2n_1^2$ [59]. The refractive index is shown in the figure(3.5). for some numerical parameters.

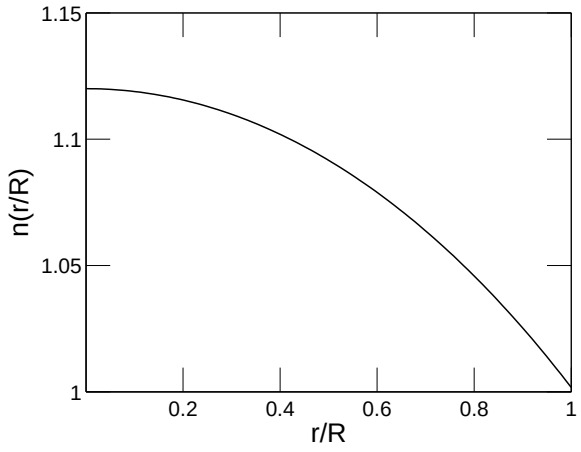


Figure 3.5: Display of index of refraction. Index of refraction of the core is displayed for some numerical values such as $n_1 = \sqrt{1+A} = 1.12$ and $n_2 = 1$.

4 LINEAR AND NONLINEAR WAVE PROPAGATION

4.1 Wave equation in dispersive media

In a dispersive media the relation between displacement current vector and electric field is given by

$$D = \epsilon(\omega)E \tag{4.1.1}$$

where $\epsilon(\omega) = \epsilon_0[1 + \chi(\omega)]$. Polarization is related to the electric field through electric susceptibility via $P = \epsilon_0\chi(\omega)E$. Susceptibility $\chi(\omega)$ is the Fourier transformation of the response function (Green function) of the medium $\chi(t)$, $\chi(\omega) = \int_{-\infty}^{\infty}\chi(t)\exp(-i\omega t)dt$. Dispersive media are characterized by frequency dependence of susceptibility. Expanding the susceptibility of the dressed atom to second order about a central frequency ω_0, and with $P(\omega-\omega_0) \equiv \epsilon_0\chi(\omega-\omega_0)E(\omega-\omega_0)$, yields[20].

$$\chi(\omega-\omega_0) = \chi(\omega_0) + \frac{\partial\chi}{\partial\omega}|_{\omega_0}(\omega-\omega_0) + \frac{1}{2}\frac{\partial^2\chi}{\partial^2\omega}|_{\omega_0}(\omega-\omega_0)^2, \tag{4.1.2}$$

which leads to the polarization[20]

$$P(t) = \epsilon_0\chi(\omega_0)E(t) - i\epsilon_0\frac{\partial\chi}{\partial\omega}|_{\omega_0}\frac{\partial E}{\partial t} - \frac{\epsilon_0}{2}\frac{\partial^2\chi}{\partial^2\omega}|_{\omega_0}\frac{\partial^2 E}{\partial^2 t}. \tag{4.1.3}$$

Maxwell equations in the medium are given by

$$\nabla\cdot\mathbf{B} = 0 \tag{4.1.4}$$

$$\nabla\cdot\mathbf{D} = \rho_{free} \tag{4.1.5}$$

$$\nabla\times\mathbf{E} = -\frac{\partial\mathbf{B}}{\partial t} \tag{4.1.6}$$

$$\nabla\times\mathbf{H} = \mathbf{J} + \frac{\partial\mathbf{D}}{\partial t} \tag{4.1.7}$$

In addition, we have the standard constitutive relations $\mathbf{D} = \epsilon\mathbf{E} + \mathbf{P}$, $\mathbf{B} = \mu_0\mathbf{H}$, $\mathbf{J} = \sigma\mathbf{E}$. In such a medium, propagation of an electromagnetic wave is determined by a wave equation in the form

$$-\vec{\nabla}^2\vec{E} + \mu_0\sigma\frac{\partial\vec{E}}{\partial t} + \frac{1}{c^2}\frac{\partial^2\vec{E}}{\partial^2 t} = -\mu_0\frac{\partial^2\vec{P}}{\partial^2 t}. \tag{4.1.8}$$

Employing the slowly varying amplitude approximation, which is described by conditions,

$$\frac{\partial \varepsilon}{\partial \mathrm{t}} \ll \omega\varepsilon \quad , \quad \frac{\partial \varepsilon}{\partial \mathrm{z}} \ll \mathrm{k}\varepsilon \tag{4.1.9}$$

$$\frac{\partial \mathcal{P}}{\partial \mathrm{t}} \ll \omega\mathcal{P} \quad , \quad \frac{\partial \mathcal{P}}{\partial \mathrm{z}} \ll \mathrm{k}\mathcal{P}. \tag{4.1.10}$$

wave equation can be reduced to

$$\frac{\partial E}{\partial z} + \alpha E + \frac{1}{v_g}\frac{\partial E}{\partial t} + i\, b_2 \frac{\partial^2 E}{\partial^2 t} = 0. \tag{4.1.11}$$

Here, the loss term α, group velocity v_g, and dispersion coefficient or the group velocity dispersion coefficient b_2 are given by [20]

$$\alpha = -\frac{i\pi}{\lambda}\chi(\omega_0), \tag{4.1.12}$$

$$\frac{1}{v_g} = \frac{1}{c} - \frac{\pi}{\lambda}\frac{\partial \chi}{\partial \omega}|_{\omega_0}, \tag{4.1.13}$$

$$b_2 = \frac{\pi}{2\lambda}\left[\frac{\partial^2 \chi}{\partial \omega^2}|_{\omega_0}\right]. \tag{4.1.14}$$

If the incident wave is a Gaussian pulse $E(0,t) = exp(-t^2/\tau_0^2)$ with width τ_0 and under the uniform density (all the coefficients are constant), we obtain analytical solution for Equation(4.1.11)[61]

$$E(z,t) = [\frac{q(0)}{q(z)}]^2 exp(i\pi\frac{(t-\tau_d)^2}{b_2 q(z)}) \tag{4.1.15}$$

Here $q(z) = z + iz_0$, $z_0 = \pi\tau_0^2/-b_2$, delay time $\tau_d = z/v_g$ and of width

$$\tau(z) = \tau_0[1 + \frac{z}{z_0}^2]^{1/2}. \tag{4.1.16}$$

In the limit $z \gg z_0$,

$$\tau(z) \approx \tau_0\frac{z}{|z_0|} = |b_2|\frac{z}{\pi\tau_0}. \tag{4.1.17}$$

When a short optical pulse enters a medium, its power is dispersed in time therefore the pulse spreads into a wider time interval. There are mainly two kind of dispersion: material dispersion and waveguide dispersion. The group velocity is defined as

$$v_g = \frac{d\omega}{dk}. \tag{4.1.18}$$

Here $\omega(k) = ck/n(k)$. We obtain for the group velocity

$$v_g = \frac{c}{n}[1 - \frac{k}{n}\frac{dn}{dk}], \tag{4.1.19}$$

or

$$v_g = \frac{c}{n + \omega\frac{dn}{d\omega}}. \tag{4.1.20}$$

4.2 Numerical scheme for ultraslow-light pulse propagation

Detailed investigation of behavior of even shorter pulses require more intensive numerical studies. Wave equation which is obtained by slowly varying amplitude approximation with time dependent initial condition is solved via finite difference Crank-Nicolson space marching scheme. The Crank-Nicolson scheme is less stable but more accurate than the fully implicit method. we discredited the Equation(4.1.11) as [58]

$$\frac{\partial E}{\partial z} = \frac{(E_j^{i+1} - E_j^i)}{\Delta z}, \tag{4.2.21}$$

$$\frac{\partial E}{\partial t} = \frac{(E_{j+1}^i - E_{j-1}^i)}{2\Delta t}, \tag{4.2.22}$$

$$\frac{\partial^2 E}{\partial^2 t} = \frac{1}{2}\frac{(E_{j+1}^i + E_{j-1}^i - 2E_j^i)}{(\Delta t)^2} + \frac{1}{2}\frac{(E_{j+1}^{i+1} + E_{j-1}^{i+1} - 2E_j^{i+1})}{(\Delta t)^2}. \tag{4.2.23}$$

Therefore Equation (4.1.11) becomes

$$\frac{(E_j^{i+1} - E_j^i)}{\Delta z} + \alpha E_j^i + \frac{1}{2v_g}\frac{(E_{j+1}^i - E_{j-1}^i)}{\Delta t}$$
$$\frac{i\,b_2}{2}\frac{(E_{j+1}^i + E_{j-1}^i - 2E_j^i + E_{j+1}^{i+1} + E_{j-1}^{i+1} - 2E_j^{i+1})}{(\Delta t)^2} = 0. \tag{4.2.24}$$

We assume a Gaussian pulse of the form $\exp(-\beta(t-t_0)^2)$ at initial time t_0, where $\sqrt{\beta}$ is the pulse width, and propagate it numerically. A dimensionless form of equation(4.1.11) is solved via finite difference Crank-Nicolson space marching scheme. We use forward difference scheme for the position and central difference scheme for the time. Discrete equations in matrix form are solved by using Thomas algorithm[58] which is analogous to a fast Gaussian elimination method for tridiagonal matrices. Wave equation is solved via finite difference Crank-Nicolson space marching scheme. The Crank-Nicolson scheme is less stable but more accurate than the fully implicit method; it takes the average between the implicit and the explicit schemes[58]. We discretized the Equation(4.1.11) and a set of linear equations are solved at each step to find E^{i+1} where i represents the position z. At each step we find E^{i+1} but this method is too slow. Accordingly, we use Thomas algorithm [58] which is equivalent than gaussian elimination method for tri-diagonal matrices.

4.3 Propagation and dispersion of ultraslow-light pulses

Probe beam propagates along the condensate axis in the z direction. We treat the axial propagation of probe beam under paraxial approximation where the paraxial effects and diffraction losses are ignored. This approximation is valid when the probe beam radius is much larger than the radial size of the atomic cloud. In practice, using a pinhole and a flipper mirror, only that portion of the probe beam passing through the thin central column region of the cloud is selectively monitored[1]. To develop a one dimensional wave equation including the high order diffraction effects in the dispersive medium for the short probe pulse, we follow reference [20].

The probe pulses we shall consider in this paper have carrier frequencies in the order of 10^{15} Hz, while their spectral widths are less than of the order of 10^{9} Hz. We will study their propagation under slowly varying phase and envelope approximations. The wave equation that would govern the propagation of a short pulse in a dispersive medium has been defined in equation(4.1.11) [20]. We have also calculated the third order dispersive coefficient b_3 and found it to be 7 orders of magnitude less than b_2 for typical experimental parameters[1]. The significant coefficients for the short pulse propagation can be calculated from the susceptibility using the relations[20]. Here we take $\lambda_{31} = \lambda$, $\omega_p \equiv \omega$ and $\omega_{31} \equiv \omega_0$ for convenient notation. It may be noted that these expressions lead to complex parameters in general, as the χ is a complex valued function and the parameters are merely mathematical coefficients in Equation4.1.11. At EIT resonance however they lead to physically meaningful, well-defined, real valued absorption coefficient, group velocity and dispersion coefficient. EIT susceptibility exhibits steep normal dispersive behavior around the resonance, which allows for the second term in Equation 4.1.13 become much larger than the first term. This leads to substantial reduction in the group velocity of the pulse. Such a slow pulse propagates through the medium without much absorption due to the small imaginary EIT susceptibility at resonance. On the other hand, for short pulses the pulse shape would also be influenced by the higher order dispersive coefficients, starting from the group velocity dispersion. Different frequency components would have different velocities and broadening of the pulse may become significant. Let us emphasize

that essential physical foundations of these effects are not related to the density ρ but the dispersive properties of the EIT susceptibility. Indeed, slow laser pulses have been observed in various media, including hot rubidium vapor[21, 22], ultracold Bose gas[1], and in solid crystals[23]. When Rabi frequency for the coupling field is sufficiently large such that $\Omega_c \gg \Gamma_{2,3}$, we can calculate these parameters characterizing propagation and dispersion of slow EIT pulses explicitly as follows

$$\alpha = \frac{2\pi\rho|\mu_{31}|^2\Gamma_2}{\epsilon_0\hbar\lambda\Omega_c^2}, \tag{4.3.25}$$

$$v_g = \frac{c\epsilon_0\hbar\Omega_c^2}{2\omega_{31}|\mu_{31}|^2\rho}, \tag{4.3.26}$$

$$b_2 = i\frac{8\pi\Gamma_3|\mu_{31}|^2\rho}{\epsilon_0\hbar\lambda\Omega_c^4}. \tag{4.3.27}$$

It should be noted that the result for v_g is valid when

$$\Gamma_{2,3} \ll \Omega_c \ll \sqrt{4\pi c|\mu_{31}|^2\rho/\epsilon_0\hbar} = \sqrt{\frac{3}{4\pi}c\lambda^3\gamma\rho}. \tag{4.3.28}$$

For $\rho \sim 10^{20} - 10^{21}\,\mathrm{m}^{-3}$, the upper limit would be $5\gamma - 15\gamma$. In this paper we consider $\Omega_c = 0.56\gamma - 5\gamma$. Corresponding electric field of the coupling laser then would be in the range $10^2 - 10^3\,\mathrm{V/m}$, with power densities $13 - 1300\ \mathrm{W/m^2}$. $\Omega_c = 0.56\gamma$ is used in typical experiments[1]. We shall discuss possible enhancement of bit storage capacity by selecting particular Ω_c within this range. According to their dependencies on the Ω_c, we see that increasing Ω_c reduces the dispersive effects significantly, but simultaneously it reduces the storage time of the pulses in the condensate as the group velocity would rise. It is illuminating to realize that decrease of delay time (storage time) is much slower than the decrease of dispersion coefficient with the Ω_c. This can be exploited to find a critical Ω_c for which number of probe pulses injected into the medium within the storage time would be optimized.

We note that for extremely large Ω_c, one should use the following expression instead

$$v_g = c\left(1 - \frac{4\pi c|\mu_{31}|^2\rho}{\epsilon_0\hbar\Omega_c^2}\right) \tag{4.3.29}$$

For a uniform density medium the equation(4.1.11) can be solved analytically[61]. An initial temporally short gaussian pulse after propagating in the medium of

length L is then found to be delayed with respect to a reference pulse propagating in vacuum by $t_d = L/v_g - L/c$. During that time, the pulse would broaden due to second-order dispersion. Leaving the medium, it would grow to a final width of

$$\tau(L) = \tau_0\sqrt{1 + (L/z_0)^2}, \tag{4.3.30}$$

with τ_0 is the initial temporal width of the pulse, and $z_0 = -\pi\tau_0^2/b_2$. For $L \gg z_0$ we get $\tau(L) = |b_2|L/\pi\tau_0$.

In general, $\rho = \rho(r, z)$ is a spatially varying function, whose profile depends on temperature, inter-atomic interactions and confinement potential. Assuming slow spatial variations within an optical wavelength the wave equation remains the same. The only effect of spatial inhomogeneity would be to give group velocity and its dispersion local character. As a result, the time delay t_d can be calculated through a spatial averaging of the group velocity field[26]. Experimentally measured group velocity is then operationally defined by $v_g = L/t_d$, where the effective axial length of the medium is evaluated by

$$L = \left[\frac{4\pi}{N}\int_0^\infty r\mathrm{d}r\int_0^\infty \mathrm{d}z z^2\rho(r, z)\right]^{1/2}. \tag{4.3.31}$$

The axial length L is an effective length corresponding to the axial width of the density distribution. It may be noted that more exact treatments can be used to determine the effective length of an interacting BEC as discussed in detail very recently[27]. There is no simple operational definition for the broadening of the pulse. One has to either determine the output pulse shape from exact numerical simulations of the wave equation or refer to uniform density results for qualitative studies. While it is the atomic density which determines the local group velocity and its dispersion, after spatial averaging, the group velocity and broadening of the pulse would become explicitly dependent on the temperature, interactions between the atoms as well as the other physical parameters due to the confinement potential. In order to elucidate these dependencies, it is necessary to define ρ concretely and discuss how it is shaped by such physical parameters. We shall specifically consider an atomic Bose-Einstein condensate as the medium of propagation in this paper and review its density profile in the next section.

4.4 Light propagation and mode dispersion

We use the cylindrical coordinate system because the refractive index profile $n(r)$ is cylindrically symmetric. If we take transverse component of the linearly polarized electric field of the (LP) modes as in reference [59]

$$E_t = \psi(r)e^{il\phi}\exp[i(\omega t - \beta_{lm}z)]. \tag{4.4.32}$$

Here $l, m = 0, 1, 2, 3, \ldots$, ϕ is the absolute phase and β_{lm} is the propagation constant in the z direction. The wave equation for the field vector field E_t is:

$$[\nabla^2 + k^2]E_t = 0. \tag{4.4.33}$$

where $k^2 = \omega^2 n^2/c^2$ and ∇^2 is the Laplacian operator in the cylindrical coordinate. The relationship between angular frequency and wave number (propagation constant in the radial direction) is:

$$\omega^2 = \frac{c^2}{n^2}(\beta_{lm}^2 \mp q^2). \tag{4.4.34}$$

Here the radial wave number $q^2 = k_x^2 + k_y^2$. If we put equation (4.4.32) in the equation (4.4.33),we will obtain:

$$[\frac{d^2}{dr^2} + \frac{1}{r}\frac{d}{dr} + p^2(r)]\psi(r) = 0, \tag{4.4.35}$$

in which $p^2(r) = k_0^2 n^2(r) - \beta_{lm}^2 - l^2/r^2$.[59] Since the refractive index does not vary appreciably over the distance on the order of one wavelength, WKB approximation may be used for solving the graded-index BEC reference [59]. In this approximation $\psi(r)$ is generally taken in the following form in order to solve equation (4.4.35).

$$\psi(r) = e^{iS(r)}, \tag{4.4.36}$$

where $S(r)$ is a complex function of r. Applying the Bohr-Sommerfeld quantization rule to the $p(r)$ [62], the mode becomes

$$\int_{r_1}^{r_2}[k_0^2 n^2(r) - \beta_{lm}^2 - \frac{l^2}{r^2}]^{1/2}dr = (m + \frac{1}{2})\pi, \tag{4.4.37}$$

Here $k_0 = 2\pi/\lambda$ and $m = 0, 1, 2, 3, \ldots$. The mode condition can be solved analytically for the propagation constant β_{lm} [59]. For the general case equation (4.4.37) becomes

$$(\frac{k_0^2 n_1^2 - \beta_{lm}^2}{(2n_1 k_0\sqrt{2\triangle})/R} - |l|)\frac{\pi}{2} = (m + \frac{1}{2})\pi. \tag{4.4.38}$$

If we solve equation (4.4.38),we obtain the propagation constant, β in the z direction which is defined as [59]

$$\beta_{lm} = n_1 k_0 [1 - \frac{2(2\triangle)^{1/2}}{n_1 k_0 R} K]^{1/2}, \tag{4.4.39}$$

where $K = (l+2m+1)$. The propagation constant β, depends on the frequency of the light. This frequency dependence determines the dispersion of the waveguide. Optical pulse waves can be dispersive because of the material used as the graded-index fiber. Propagation constant is defined in terms of mode index $\beta_{lm} = n_{lm} k_0 = n_{lm}(n_1, n_2, \omega)\omega/c$. The group velocity v_g is defined as

$$\frac{1}{v_g} = \frac{d\beta_{lm}}{d\omega} = \frac{\omega}{c}(\frac{\partial n_{lm}}{\partial n_1}\frac{\partial n_1}{\partial \omega} + \frac{\partial n_{lm}}{\partial n_2}\frac{\partial n_2}{\partial \omega} + \frac{\partial n_{lm}}{\partial \omega}) + \frac{n_{lm}}{c}. \tag{4.4.40}$$

Here, the first two terms in the square bracket are the contribution from material dispersion, the third term is waveguide dispersion [59]. Therefore the group velocity is characterized by

$$v_g = \frac{c}{n_{lm} + \omega\frac{\partial n_{lm}}{\partial n_1}\frac{\partial n_1}{\partial \omega} + \omega\frac{\partial n_{lm}}{\partial n_2}\frac{\partial n_2}{\partial \omega} + \omega\frac{\partial n_{lm}}{\partial \omega}}. \tag{4.4.41}$$

Here c is the speed of the light in the free space.

4.5 Numerical scheme for optical waveguiding

More accurate results may be obtained using a numerical scheme in order to solve Equation 4.4.35. For that purpose it is assumed that the index of refraction increases incrementally from the edge to the center of the core. If the number of increments is high enough, this model will be a faithful representation of the conditions prevailing in the inhomogeneous core. If the turning point is in the interval m then the solution of the equation(4.4.35) in the interval $i < m$ will be

$$\psi = A_i J_l(q_i r) + B_i Y_l(q_i r) \tag{4.5.42}$$

where J_l , Y_l are Bessel functions of the first and second kind of order l. q_i is $\sqrt{\omega^2 n_i^2/c^2 - \beta^2}$. n_i is the index of refraction in the interval i. For $i > m$, the index of refraction is lower than that of the turning point and accordingly the solution of the wave equation becomes

$$\psi = A_i I_l(q_i r) + B_i K_l(q_i r) \tag{4.5.43}$$

where I_l, K_l are modified Bessel functions of the first and second kind. In that case q_i is $\sqrt{-\omega^2 n_i^2/c^2 + \beta^2}$. The boundary conditions are $B_0 = 0$ (The wave is bounded at the origin) and $A_{N+1} = 0$ (the wave does not diverge at infinity.)

The function ψ and its radial derivative is continuous. This continuity provides a recurrence relation between successive coefficients A_i, B_i. For $i < m$ the recurrence relation is more stable for increasing m. The coefficients A_m and B_m at the turning point may be calculated from A_0 or alternatively they may be derived from B_N+1. In both derivations the ratio A_m/B_m must have the same value. The preservation of this ratio provides an equation for the wave number β.

4.6 Nonlinear wave propagation

We will study propagation of short pulses under slowly varying phase and envelope approximations in nonlinear regime. The wave equation that would govern the propagation of a short pulse in a dispersive medium can be found to be. Total polarization is related to the electric field through electric susceptibility via $\mathbf{P} = \mathbf{P^{(l)}} + \mathbf{P^{(nl)}}$ where $\mathbf{P^{(l)}} = \epsilon_0 \chi(\omega)^{(1)}\mathbf{E}$ and $\mathbf{P^{nl}} = \epsilon_0(\chi(\omega)^{(2)} : \mathbf{EE} + \chi(\omega)^{(2)} : \mathbf{EEE})$. Dispersive media are characterized by frequency dependence of susceptibility. Expanding the linear susceptibility $\chi^{(1)}$ of the dressed atom to second order about a central frequency ω_0, and with the nonlinear term

$$\begin{aligned} P(\omega - \omega_0, E) &= \epsilon_0 \chi(\omega - \omega_0)^{(1)} E(\omega - \omega_0) \\ &+ \epsilon_0 \chi^{(2)} : \mathbf{EE} + \epsilon_0 \chi^{(3)} : \mathbf{EEE}, \end{aligned} \tag{4.6.44}$$

where linear susceptibility is defined as

$$\begin{aligned} \chi(\omega - \omega_0)^{(1)} &= \chi(\omega_0) + \frac{\partial \chi}{\partial \omega}|_{\omega_0}(\omega - \omega_0) \\ &+ \frac{1}{2}\frac{\partial^2 \chi}{\partial^2 \omega}|_{\omega_0}(\omega - \omega_0)^2, \end{aligned} \tag{4.6.45}$$

which leads to the polarization[20]

$$\begin{aligned} P(t) &= \epsilon_0 \chi(\omega_0)^{(1)} E(t) - i\epsilon_0 \frac{\partial \chi^{(1)}}{\partial \omega}|_{\omega_0}\frac{\partial E}{\partial t} \\ &- \frac{\epsilon_0}{2}\frac{\partial^2 \chi^{(1)}}{\partial^2 \omega}|_{\omega_0}\frac{\partial^2 E}{\partial^2 t} \\ &+ \epsilon_0 \chi^{(2)} : \mathbf{EE} + \epsilon_0 \chi^{(3)} : \mathbf{EEE}. \end{aligned} \tag{4.6.46}$$

In slowly varying approximation scheme, maxwell wave equation is written as

$$\frac{\partial E}{\partial z} + \frac{1}{c}\frac{\partial E}{\partial t} = \frac{ik}{2\varepsilon_0}P. \tag{4.6.47}$$

If we use equation(4.6.46) in equation(4.6.47), we will get nonlinear wave equation for the optical pulse.

$$\frac{\partial E}{\partial z} + \alpha E + \frac{1}{v_g}\frac{\partial E}{\partial t} + i\, b_2 \frac{\partial^2 E}{\partial t^2} + i\eta |E|^2 E = 0, \tag{4.6.48}$$

where α determines the pulse attenuation; v_g is the group velocity, b_2 is the second-order dispersion coefficient, or the group velocity dispersion, and η is the nonlinear optical Kerr coefficient. We have also calculated the third order dispersive coefficient b_3 and found it to be 7 orders of magnitude less than b_2 for typical experimental parameters[1]. The coefficients above for the short pulse propagation can be calculated from the susceptibility

$$\alpha = -\frac{i\pi}{\lambda}\chi(\omega_0), \tag{4.6.49}$$

$$\frac{1}{v_g} = \frac{1}{c} - \frac{\pi}{\lambda}\frac{\partial \chi}{\partial \omega}|_{\omega_0}, \tag{4.6.50}$$

$$b_2 = \frac{\pi}{2\lambda}\left[\frac{\partial^2 \chi}{\partial \omega^2}|_{\omega_0}\right], \tag{4.6.51}$$

$$\eta = -\frac{\pi}{\lambda}\chi^{(3)}(\omega_0). \tag{4.6.52}$$

Here we take $\lambda_{31} = \lambda$, $\omega_p \equiv \omega$ and $\omega_{31} \equiv \omega_0$ for convenient notation. It may be noted that these expressions lead to complex parameters in general, as the χ is a complex valued function and the parameters are merely mathematical coefficients in equation(4.6.48). At EIT resonance however they lead to physically meaningful well-defined real valued absorption coefficient, group velocity and dispersion coefficient. When Rabi frequency for the coupling field is sufficiently large such that $\Omega_c \gg \Gamma_{2,3}$, we get

$$\alpha = \frac{2\pi\rho|\mu_{31}|^2\Gamma_2}{\epsilon_0\hbar\lambda\Omega_c^2}, \tag{4.6.53}$$

$$v_g = \frac{c\epsilon_0\hbar\Omega_c^2}{2\omega_{31}|\mu_{31}|^2\rho}, \tag{4.6.54}$$

$$b_2 = i\frac{8\pi\Gamma_3|\mu_{31}|^2\rho}{\epsilon_0\hbar\lambda\Omega_c^4}, \tag{4.6.55}$$

$$\eta = i\frac{4\rho|\mu_{31}|^4\Gamma_2}{3\varepsilon_0\hbar^3\Gamma_3}\frac{(\Gamma_2+\Gamma_3)}{\Omega_c^4}. \tag{4.6.56}$$

It should be noted that the result for v_g is valid when

$$\Gamma_{2,3} \ll \Omega_c \ll \sqrt{4\pi c|\mu_{31}|^2\rho/\epsilon_0\hbar} = \sqrt{\frac{3}{4\pi}c\lambda^3\gamma\rho}. \tag{4.6.57}$$

$\chi^{(2)}$ is finite only for asymmetric systems. Our system (BEC) is symmetric so second harmonic ,$\chi^{(2)}$ is zero.

4.7 Transmission with electromagnetically induced transparency

In the ideal EIT medium with resonant control field, transmitivity is given by[7]

$$\Delta\omega_{trans} = \frac{\Omega_c^2}{\sqrt{\Gamma_3\gamma}}\frac{1}{\sqrt{\rho\sigma z}}. \tag{4.7.58}$$

Here ρ is the peak density of the Bose-Einstein condensate, $\sigma = 3\lambda^2/2\pi$ is the absorption cross section of an atom, and z is the length of the medium.

5 RESULTS AND DISCUSSION

5.1 Dispersive effects on BEC

Let us first compare the relative strength of the last two terms of the wave equation. The third term describes the group velocity dispersion while the last (fourth) one is for the second order dispersion. We have analytically calculated the second order dispersion coefficient b_2. Substituting the numerical values taken from experiment[1], where $a_s = 2.75\,\mathrm{nm}$, $\omega_r = 2\pi \times 69\,\mathrm{Hz}$,$\omega_z = 2\pi \times 21\,\mathrm{Hz}$, we numerically evaluated it to be in the order of $b_2 \sim 10^{-9}\,\mathrm{s}^2/\mathrm{m}$ about the center of a ^{23}Na condensate with the total number of atoms $N = 8.3 \times 10^6$. For some other set of experimentally accessible parameters we have found $b_2 \sim 10^{-8}\,\mathrm{s}^2/\mathrm{m}$. We have also checked third order dispersion coefficient and have found it $\sim 10^{-15}\,\mathrm{s}^3/\mathrm{m}$, which is insignificant. Taking the ratio of the third term to the fourth term, we find that the condition for dispersion to be significant is $(\tau/V_G) \times 10^9 \ll 1$, where τ denotes the temporal pulse width . Subluminal light speeds achieved using ^{23}Na BECs are in the order of $1-100(\mathrm{m/s})$. This yields $\tau \ll 10^{-8}$. This explains clearly laser pulses used in present slow-light experiments in condensates do not suffer from dispersion. They are however not the optimal choice for a higher capacity optical memory. One could use a ten times shorter pulse so that $\tau \sim 10^{-7}$. Such a pulse would be influenced by little dispersion in the condensate and would be an optimal choice to use in optical memories. We present our numerical simulation results in Figs.5.1-5.2 for the propagation of pulses of widths 10^{-6}s and 10^{-7}s, respectively. In the figures we use dimensionless scaled position (z) and time variables. Position is scaled by the condensate radius while time is scaled by the pulse width. Diameter of the BEC is $\sim 50\,\mu$m. Effect of second order dispersion is a small broadening in the temporal pulse width as demonstrated in Figure(5.2), where, behavior of the pulse about the center of the condensate, where the dispersive effects are most influential, is shown.[50]

In our numerical calculations of the theoretical results presented in the preceding

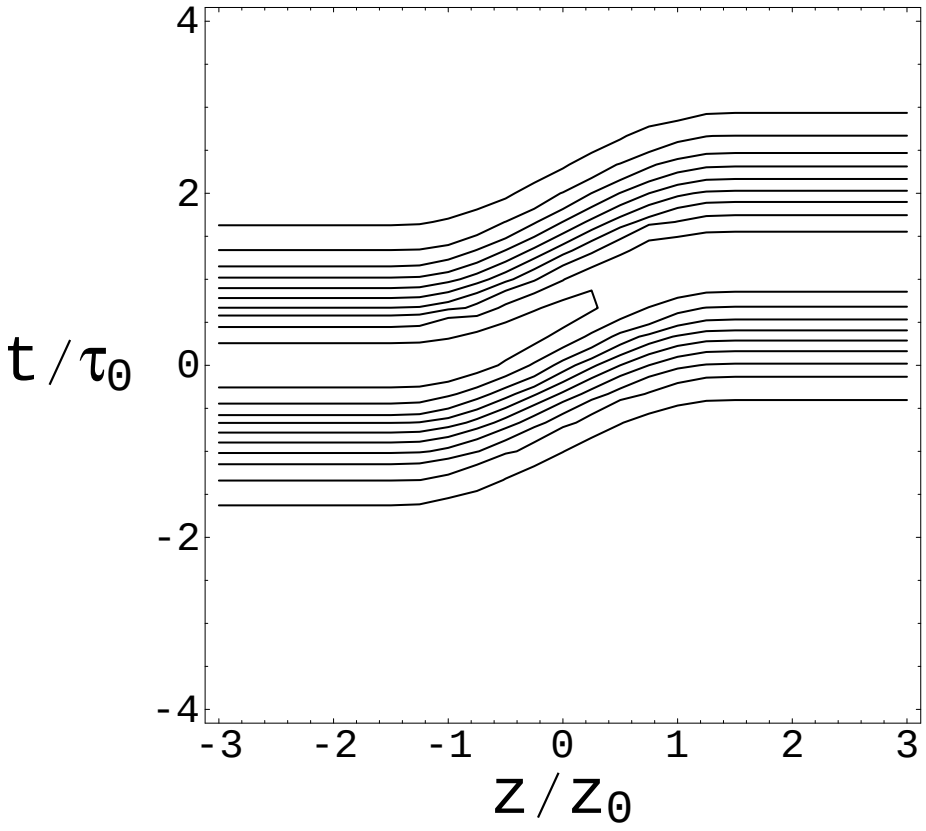


Figure 5.1: Contour plot of the propagation of pulse width $\tau = 10^{-6}$s. Contour plot of the propagation of an EIT pulse of width $\tau = 10^{-6}$s through a ^{23}Na BEC is displayed and time and position are in dimensionless units as explained in the text.

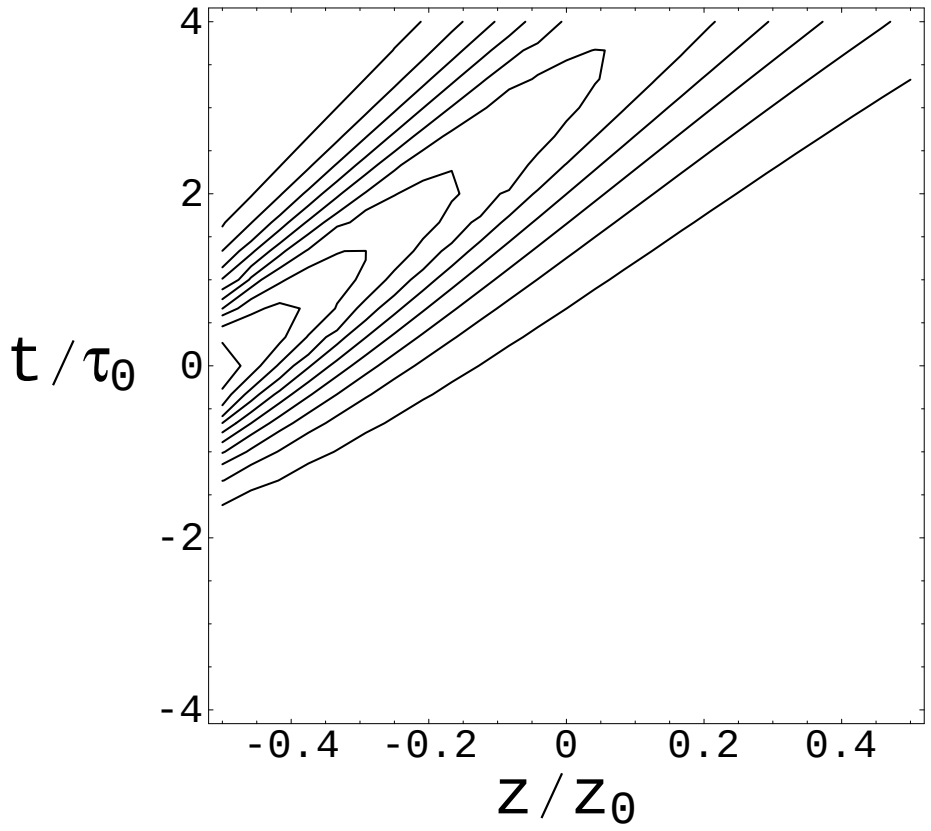


Figure 5.2: Contour plot of the propagation of pulse width $\tau = 10^{-7}$s. Contour plot of the propagation of an EIT pulse of width $\tau = 10^{-7}$s through a ^{23}Na BEC is shown and time and position are in dimensionless units as explained in the text.

section, we shall specifically consider a gas of $N = 8.3 \times 10^6$ ^{23}Na atoms for which $M = 23$ amu, $\lambda_0 = 589$ nm, $\gamma = 2\pi \times 10.01$ MHz, $\Gamma_3 = 0.5\gamma$, $\Gamma_2 = 2\pi \times 10^3$ Hz, and $a_s = 2.75$ nm. For the parameters of the trapping potential, we take $\omega_r = 2\pi \times 69$ Hz and $\omega_z = 2\pi \times 21$ Hz as in reference [1]. The coupling field Rabi frequency is taken to be $\Omega_c = 0.56\gamma$[1]. Critical temperature for Bose-Einstein condensation of such a gas is found to be $T_C = 424$ nK. We illustrate the spatial density profile of the condensate in the axial (z) direction at $T = 43$ nK in figure.(5.3).

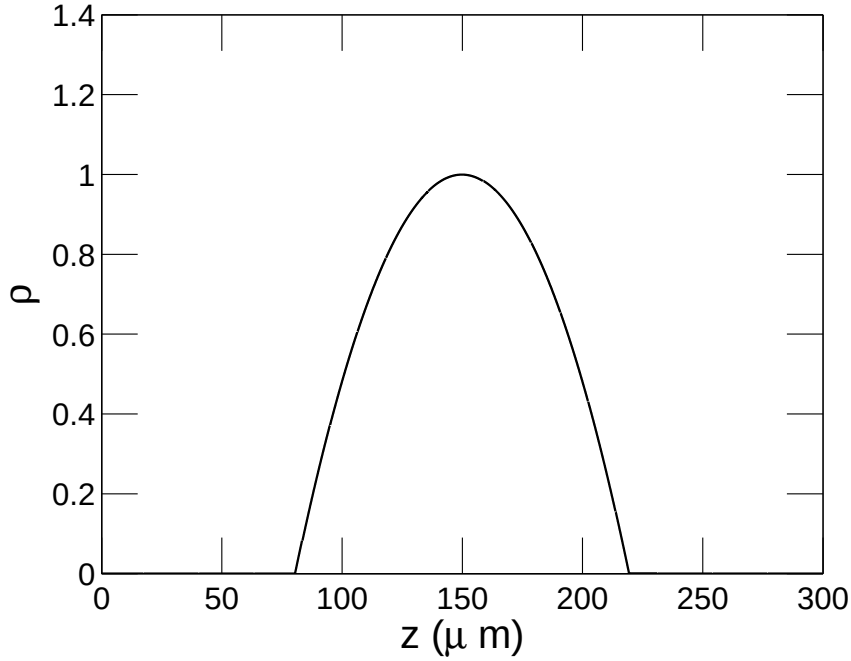


Figure 5.3: Axial density profile of BEC. Axial density profile of ^{23}Na the Bose-Einstein condensate of $N = 8.3 \times 10^6$ atoms at $T = 43$ nK. ρ is scaled by the peak density. Trap parameters are chosen to be $\omega_r = 2\pi \times 69$ Hz and $\omega_z = 2\pi \times 21$ Hz.

Due to spatially inhomogeneous density, the linear dielectric susceptibility would also be spatially inhomogeneous. In this case, group velocity defined by equation(4.6.54) would have a local character. Under EIT conditions, when the light pulse enters the condensate from the thermal component of the gas, its group speed exhibits a dramatic slowing down as shown in figure(5.4). Here we consider resonant probe pulse with $\Delta = 0$. Within the condensate region, at such low temperatures, the group velocity remains roughly at the same ultraslow value. The pulse rapidly accelerates to high speeds when it leaves the condensate at the interface to thermal component. Before and after the thermal component,

the pulse is assumed to be propagating in vacuum. In practice, group velocity is measured in terms of time delay of the pulse with respect to a reference pulse propagating in vacuum over the same distance with the gas. To make comparisons with this operational definition of the group velocity, one needs to make careful spatial averaging of the theoretical group velocity[26].

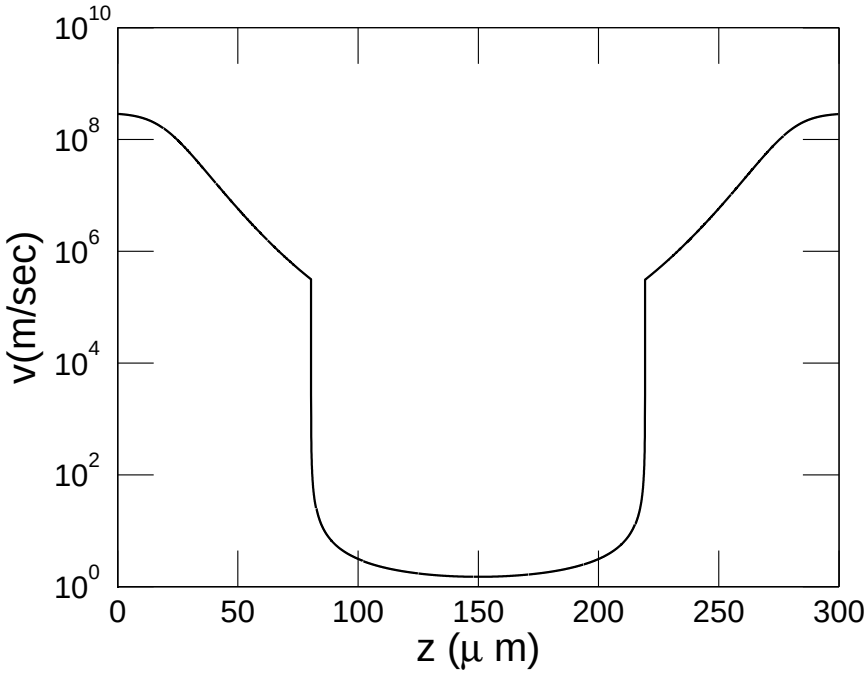


Figure 5.4: Spatial dependence of group velocity. Spatial dependence of the local group velocity of a resonant probe pulse along the z-axis, with $\Delta = 0$, propagating through a ^{23}Na the Bose-Einstein condensate of $N = 8.3 \times 10^6$ atoms at $T = 43$ nK under EIT scheme. The parameters used are $M = 23$ amu, $a_s = 2.75$ nm, $\lambda_0 = 589$ nm, $\gamma = 2\pi \times 10.01$ MHz, $\Gamma_3 = 0.5\gamma$, $\Omega_c = 0.56\gamma$, $\Gamma_2 = 2\pi \times 10^3$ Hz.

The other coefficients in the wave equation are also locally defined. The coefficient of absorption and the second-order dispersion coefficient are shown in figure(5.5) and in figure(5.6), respectively. Under EIT conditions, imaginary part χ'' of χ is small, despite the large condensate density. For large Ω_c we have $\chi'' \sim \rho\Gamma_2/\Omega_c^2$. For short pulse propagation we shall see that the major source of reduction in the peak of the pulse would be the temporal broadening due to dispersion. The absorption over the small size of the BEC is negligibly small. Taking $\alpha = 10^3\,\mathrm{m}^{-1}$ and $L = 100\,\mu$m, we can roughly estimate attenuation of the pulse by $\exp(-\alpha L)$, which yields about 90% transmission. The loss term can be made smaller by using larger Rabi frequencies for the coupling control field. The positive sign of α reflects

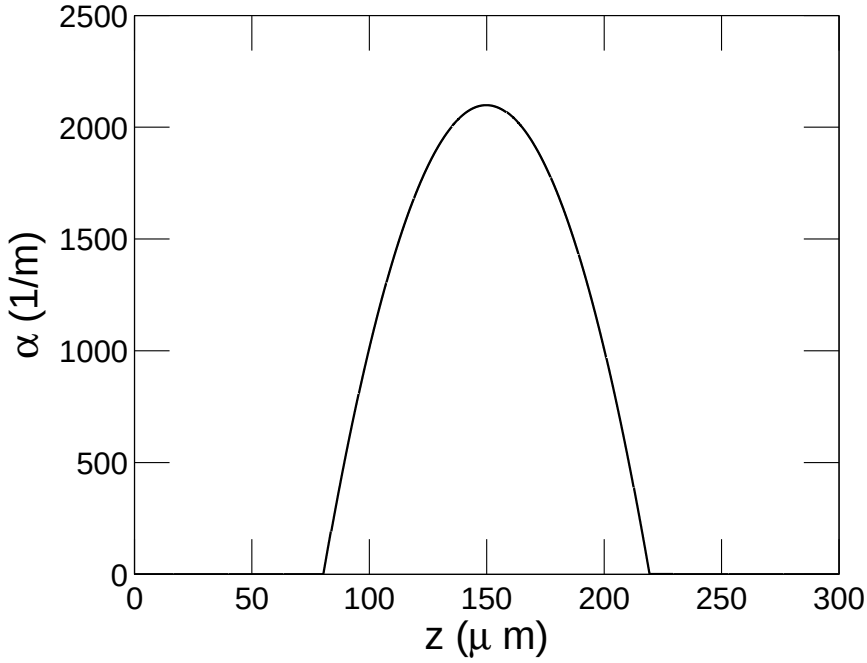


Figure 5.5: The absorption coefficient. Position dependence of the absorption coefficient α along the z-axis is displayed. The parameters are the same with those of figure(5.4)

its effect on the pulse as the decrease of the pulse intensity. The broadening of the pulse on the other hand is independent of the sign of b_2, as can be deduced from equation(4.3.30).

The region over which dispersive effects are most strong is a small region near the center of the cloud as can be seen in figure(5.6). The size of this region can be determined by the width L of the density distribution, since b_2 is proportional to ρ. It is quite smaller than the classical boundary $\sqrt{2\mu/m\omega_z^2}$. As an example, $L \approx 26\,\mu$m in figure(5.3), while the condensate is extended over a size of $\sim 140\,\mu$m. In such a small region, spatial variations of ρ can be ignored so that $\rho \approx \rho(r = 0, z = 0) \equiv \rho_0$. When a pulse of width τ_0 enters into this strongly dispersive zone, its final width would approximately broaden to $\tau(L) = \tau_0\sqrt{1 + \kappa^2(\rho_0 L)^2/\tau_0^4}$, where $\kappa = 3\Gamma_3\gamma\lambda^2/\pi^2\Omega_c^4$. Broadening of the pulse depends on the density profile of the medium through its characteristic parameters, its peak value ρ_0, and its width L. For small dispersion, change in the pulse width would be proportional to $(\rho_0 L)^2$. For the given ρ within the semi-ideal model, L demonstrates the well-known temperature variation[28] as shown

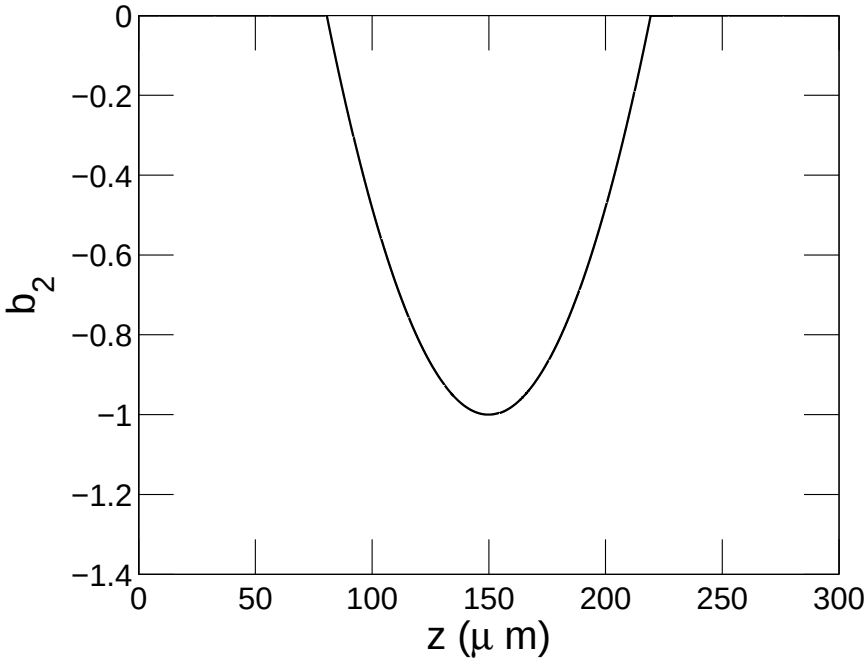


Figure 5.6: Second-order dispersion coefficient. Axial spatial profile of the second-order dispersion coefficient b_2 for the parameters same with those of figure(5.4). Vertical axis is scaled by the peak value of b_2 which is ~ 0.108 s$^2/nm$.

in figure(5.7). At a given temperature, L has been evaluated by equation(4.3.31). At very high temperatures, $T \gg T_C$, classical thermal radius would be $\sim \sqrt{T}$ according to the equipartition theorem. In the temperature range of figure(5.7), beyond T_C, L is changing linearly with T. It might be illuminating to rewrite equation(4.3.31) as $L = \sqrt{(4\pi/N)(\langle z^2\rangle_C + \langle z^2\rangle_T)}$. Here, $\langle z^2\rangle_{C,T}$ stands for a mean square axial distance evaluated using either condensate (C) or thermal density (T) distribution. The sharp drop of the width of the distribution just below T_c is due to the emergence of condensed component with relatively high density about the center of the cloud. As T becomes lower, thermal component shrinks, while the condensate part expands slowly about the center of the cloud. L eventually saturates down to Thomas-Fermi width at zero temperature. The thermal behavior of the peak density is also well-known[29, 28]. At high temperatures it shows $\sim 1/T^{3/2}$ decay consistent with classical gas behavior. Just below T_C, ρ_0 grows rapidly due to emerging relatively dense condensate about the center of the cloud. At extremely low temperatures, ρ_0 saturates to Thomas-Fermi density.

Figure(5.8) describes dependence of broadening on temperature and interatomic

interaction. At extremely low temperatures, L and ρ_0 are determined by the condensate part and they change slowly with T. For increasing T, thermal part expands beyond the boundaries of the condensate, so that L will be contributed significantly by the thermal part. Except at temperatures close to T_C, ρ_0 is dominated by the condensate part, which exhibits slow dependence on T in comparison to that of L. As a result, the product $\rho_0 L$ grows, following the expansion of thermal component, up to a point just below T_C, where ρ_0 dramatically drops to dilute thermal density value due to rapid disappearance of the dense condensate component. After that peak point, ρ_0 shows faster variation with T relative to that of L. Hence, the shape of broadening curve is characterized by the thermal behavior of ρ_0. At temperatures higher than T_C, broadening decreases with temperature. At such high temperatures, L grows slowly (almost linear) while ρ_0 decreases like $1/T^{3/2}$. Thus their product becomes a decreasing function with T. Summarizing, the broadening is determined by the density profile through its characteristic product $\rho_0 L$. As ρ_0 and L exhibit competing thermal behaviors, a peak arises just before the T_C, a signature of emerging condensate being a strongly dispersive region. Before the peak point, it is L which shapes the temperature dependence of the broadening. After the peak point, broadening behaves analogous to the thermal behavior of ρ_0.

Earlier studies indicate that group velocity depends on the strength of atomic interactions within the condensate which is characterized by the s-wave scattering length a_s. As the a_s grow longer, the group velocity of the pulse within the BEC becomes faster[35]. In order to discuss the influence of atomic interactions on broadening of the pulse, we first note that below T_C the atomic energies are so low that, there is only a_s, s-wave scattering length, to characterize the strength of interactions within the condensate component. At higher temperatures beyond T_C, the interactions has no effect within the semi-ideal model where thermal gas is dilute and non-interacting. In figure(5.8), we see that as the a_s increases, the broadening decreases when $T < T_C$. According to semi-ideal model density profile, we get $\rho_0 = \mu/U$ at $T < T_C$, from which we conclude $\rho_0 \sim 1/a_s^{3/5}$. This is intuitively expected, as the increase of repulsive atomic interactions results in lower densities. The width of the atomic cloud would slightly increase with a_s.

The increase of the size of the condensate can be estimated from the Thomas-Fermi axial radius given by $\sqrt{2\mu/m\omega_z^2} \sim a_s^{1/5}$. Thus, we see that the increase of L would be slower than the decrease of the ρ_0, so that $\rho_0 L$ and hence the broadening would reduce with a_s. This conclusion remains the same at higher temperatures where the thermal length scale becomes dominant in determining L, and it is not influenced by a_s. Thus, broadening decreases due to decrease of ρ_0. Beyond T_C, the density profile is semi-classically determined and is independent of a_s. The semi-ideal model density profile becomes not as good description of the condensate when the interactions characterized by the scaling parameter s becomes larger than 0.4, corresponding to $a_s \sim 7$ nm. For ^{23}Na cloud, $a_s = 2.75$ nm. The higher a_s may be achieved by utilizing Feshbach resonance technique[37, 38, 39] or by considering alternative atoms.

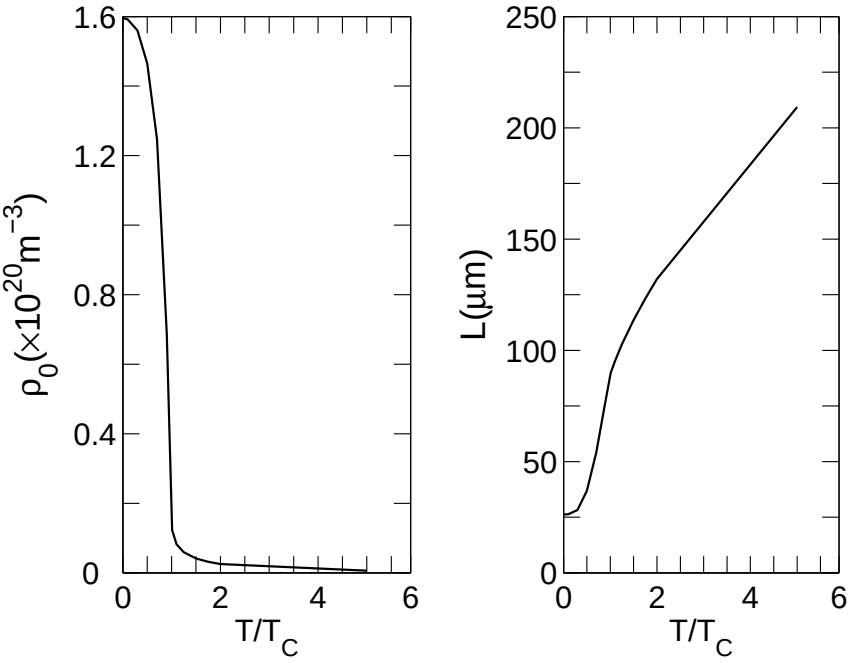


Figure 5.7: Thermal behavior of the ρ_0 and the effective axial length L. Thermal behavior of the peak ρ_0 and the effective axial length L of the atomic density distribution, given by the semi-ideal model are shown. The parameters are the same with those of figure(5.4).

Our approach in determining the pulse broadening using the effective medium width L , as we will show below, gives qualitatively accurate behavior of the broadening but overestimates it. In an actual pulse propagation, a pulse of width

τ_0 would be prepared far from the gaseous medium. Before reaching to the most dispersive zone about the center of the cloud, the pulse would pass through the thermal cloud and then through the edges of the condensate. Due to the inhomogeneous density profile, when the pulse arrives to the center of the cloud, it would already be much broader than τ_0. As a result it would suffer less from dispersion than the one predicted above. Despite the lack of actual input value τ_0 for our analysis above, the overall qualitative behavior is expected to be accurate. To test this expectation and to justify our effective central dispersive zone treatment agree qualitatively with the exact pulse behavior, we now investigate the variation of the pulse width with distance of propagation, taking into account the full spatially inhomogeneous density profile of the gaseous medium.

We have performed extensive numerical simulations at various T and confirmed that despite being an overestimation, the qualitative behavior predicted in figure(5.8) correctly describes the results obtained by the exact solution. We present typical results of our simulations in Figs.5.10-5.12. For a nanosecond pulse, at $T = 43\,\mathrm{nK}$, broadening is $\sim 3\,\mu\mathrm{s}$ which can be seen in figure(5.9). This is much smaller than the result found by the uniform density calculation, which gives $\sim 100\,\mu\mathrm{s}$ at the same temperature in figure(5.8). More moderate broadening is obtained for a pulse of width $0.1\,\mu\mathrm{s}$ and shown in figure(5.11). As a rule of thumb, we assume that broadening is not significantly large if it is less than a factor of 2. A microsecond pulse broadens by a factor of ~ 1.7 as can be seen in figure(5.12). For longer pulses therefore we conclude that broadening is not significant.

In early ultraslow light experiments microsecond pulses were used[1]. Previous theoretical models ignore dispersion effects in the pulse propagation. While they can be used to describe observed group velocities, they cannot explain the transmitted pulse shape adequately. High-order dispersion, absorption, transverse diffraction, and off-resonant transitions to upper levels not included in the three-level model cause imperfect transition, and result in reduction of the transmitted peak intensity. We have already argued that absorption, though still present even under EIT conditions, makes a little effect over the small BEC size. Transverse diffraction due to paraxial pulse propagation is also not too strong[35]. To

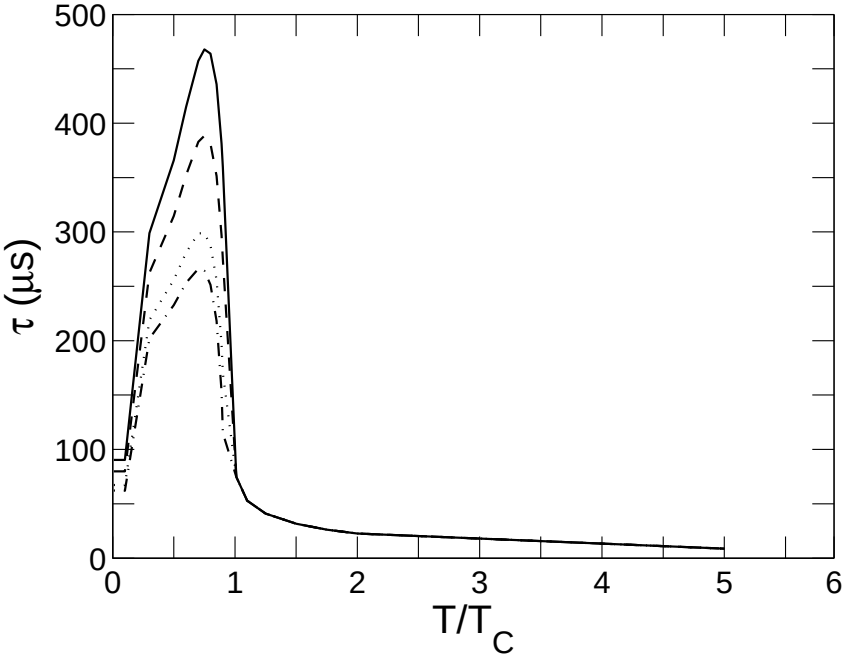


Figure 5.8: Thermal behavior of the broadening of a nanosecond pulse obtained analytically by an effective dispersive zone treatment. The solid, dashed, dotted and dot-dashed lines are for $a_s = 2.75, 3.75, 5.75$ nm, and $a_s = 7$ nm, respectively. The other parameters are the same with those of figure(5.4) [51, 54].

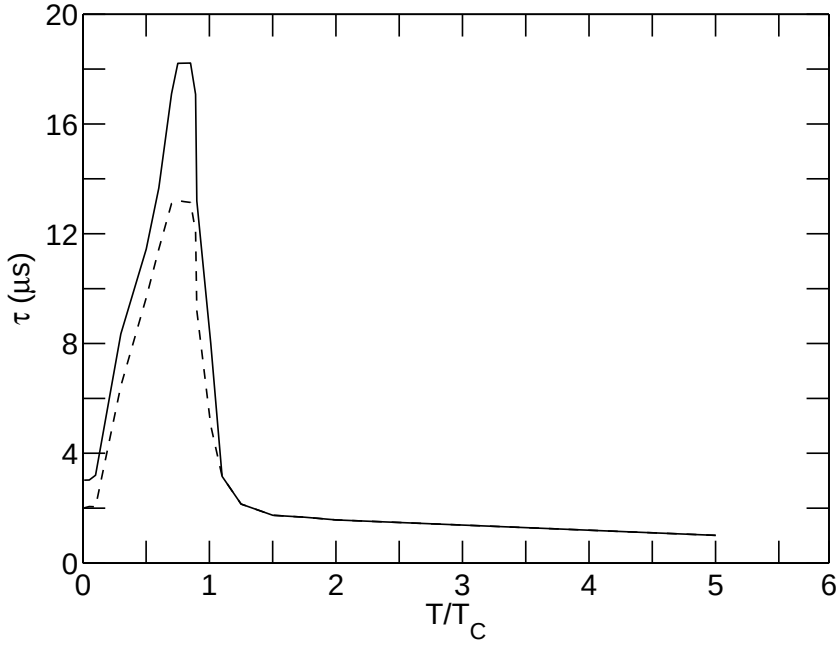


Figure 5.9: Thermal behavior of the broadening of a nanosecond pulse determined by numerical simulations. The solid and dashed lines are for $a_s = 2.75$ nm and $a_s = 7$ nm, respectively. The other parameters are the same with those of figure(5.4) [51, 54]

characterize the contribution of second-order dispersion on the reduction of the peak intensity, propagation of a microsecond pulse is simulated and presented in figure(5.12). This result indicates that in addition to off-resonant transitions to other levels, broadening of the pulse also contributes to the observed drop of the transmitted peak intensity. [51]

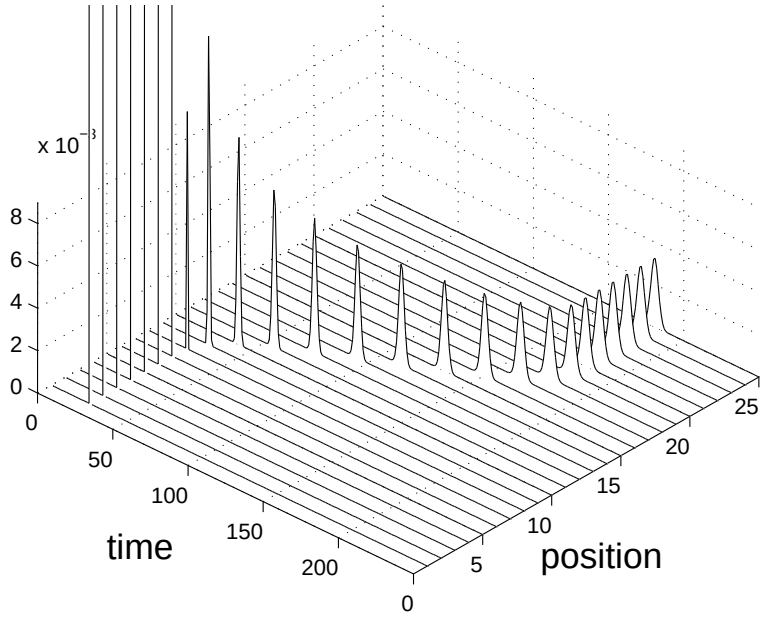


Figure 5.10: Propagation of a nanosecond pulse through the interacting BEC. Time (t) is scaled by $0.4\,\mu$s. and position (z) is by $10\,\mu$m. The parameters are the same with those of figure(5.4) [51, 54].

While microsecond pulses are good to minimize dispersive effects, shorter pulses may be more attractive for optical information processing. The question we would like to now address is if such shorter pulses can still be stored as efficiently via EIT scheme in atomic ultracold gases. We may characterize coherent optical information storage capacity through a parameter given by $C = L/2v_g\tau(L)$. It measures number of probe pulses simultaneously present in BEC without significant overlap. The storage time is taken to be the delay time of the pulses, $t_s = L/v_g$. We choose an ideal repetition rate of the pulse train to be $1/2\tau(L)$. The pulses are assumed to be stored in the central region of the cloud, whose length L is given by equation(4.3.31). It is the same with the effective central dispersive zone considered in the analytical broadening calculation. In this region $\rho \approx \rho_0$ is ap-

proximately uniform at its peak value, leading to spatially homogeneous v_g, that can be seen in figure(5.4). More explicitly, C becomes

$$C = \frac{L}{2\tau_0\sqrt{4\pi^2\Omega_c^4/9\lambda^4\gamma^2\rho^2 + 4L^2\Gamma_3^2/\pi^2\tau_0^4\Omega_c^4}}. \tag{5.1.1}$$

The second term under the square root in the denominator represents the second-order dispersive contribution. When dispersion is not too strong, C could be made higher by increasing ρ. On the other hand, it is not very simple task to increase ρ for BEC. Besides, it implicitly and indirectly affects the dispersive term via L. For a given τ_0, more explicit and direct control parameter would be Ω_c. C exhibits a non-trivial dependence on Ω_c, which is illustrated in figure(5.13). We observe that for given atomic cloud, and τ_0, there is an optimum choice of Ω_c. figure(5.13) also compares C for different τ_0. We deduce that, for a wide range of Ω_c it is indeed possible to inject more pulses by using shorter τ_0. However, reducing τ_0 from $1\,\mu$s to $0.01\,\mu$s, one cannot hope to increase the capacity 100 times more. Instead, due to dispersive effects, only by using a critical coupling laser Rabi frequency, storage capacity can be made maximum. The maximum achievable capacity C_{max} is independent of τ_0, and is found to be

$$C_{max} = \sqrt{\frac{3\gamma\lambda^2 L\rho}{32\Gamma_3}}, \tag{5.1.2}$$

which is evaluated at the critical coupling Rabi frequency, Ω_{c0}, given by

$$\Omega_{c0} = \left(\frac{3\Gamma_3\lambda^2\gamma\rho L}{\pi^2\tau_0^2}\right)^{1/4}. \tag{5.1.3}$$

These results suggest that shorter pulses can be stored in the cloud as efficiently as microsecond pulses. The storage time t_{s0} when $\Omega_c = \Omega_{c0}$ becomes

$$t_{s0} = \tau_0\left(\frac{\sqrt{3}\lambda\sqrt{\gamma}}{2\sqrt{\Gamma_3}}\right)\left(\sqrt{\rho L}\right). \tag{5.1.4}$$

We note that analytical result of C underestimates the actual value of it, as $\tau(L)$ is overestimated. Due to spatial inhomogeneity, τ_0, pulse width just before the central zone, would be larger than the width of the original pulse prepared away from the atomic cloud, so that $\tau(L)$ would be smaller. v_g would remain the same under any pulse width change. As a result, actual C would be higher than the

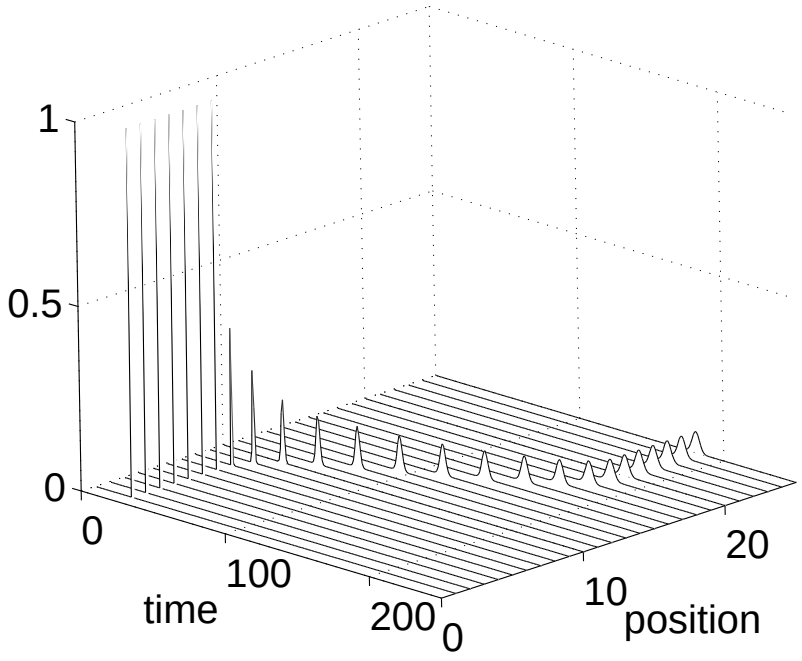


Figure 5.11: Propagation of a pulse of width $0.1\,\mu$s through the interacting BEC. Time (t) is scaled by $0.4\,\mu$s. and position (z) is by $10\,\mu$m. The parameters are the same with those of figure(5.4).

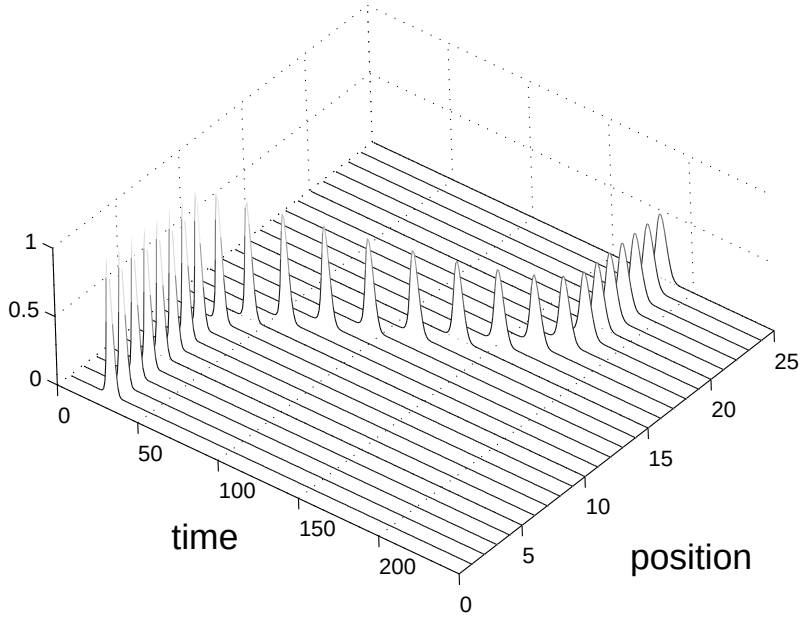


Figure 5.12: Propagation of a microsecond pulse through the interacting BEC. Time (t) is scaled by $0.4\,\mu$s. and position (z) is by $10\,\mu$m. The parameters are the same with those of figure(5.4) [51, 54].

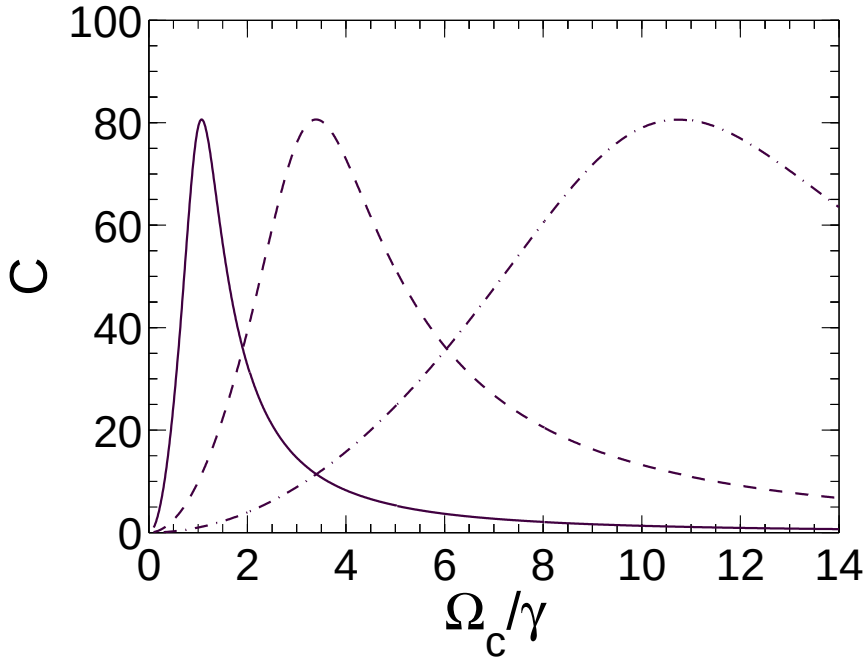


Figure 5.13: Coherent optical information storage capacity C (dimensionless) as a function of coupling field Rabi frequency Ω_c, scaled by γ. Parameters used are $L = 100\,\mu$m, $\tau_0 = 1\,\mu$s (solid line), $\tau_0 = 0.1\,\mu$s (dashed line), $\tau_0 = 0.01\,\mu$s (dot-dashed line), $\rho = 10^{21}\,\mathrm{m}^{-3}$. The other parameters are the same with those of figure(5.4) [51, 54].

one predicted above. The analytical expressions are mainly good for predicting qualitative behavior of C with Ω_C, and providing a lower limit for its value. [51, 52]

5.2 Ultraslow optical waveguiding in BEC

We investigate ultraslow waveguiding by BEC under EIT conditions. By considering slightly off-resonant EIT pulses propagating in a BEC, tightly trapped in transverse dimensions, possibility of weakly guided regime with few modes is shown. Single mode condition is established. Thermal behavior of the number of optical modes that can be supported by the BEC will be shown. Group speeds of each mode will be determined, taken into account EIT dispersion as well as the waveguide dispersion. Mode patterns will be studied numerically. Under EIT conditions, in equation(4.4.41) when we compare waveguide dispersion with the material dispersion, material dispersion is much bigger than the waveguide dispersion, therefore we can neglect waveguide dispersion term. Mode index n_{lm} is equal to 1.01968 under EIT scheme, so we can take it as 1. The dependence of β on mode indices l, m causes the different modes to have phase velocities $v_p = \omega/\beta_{lm}$ as well as group velocities $v_g = d\omega/d\beta_{lm}$ [59]. Above existing circumstances, we can define the group velocity as,

$$v_g = \frac{c}{1 + \omega \frac{\partial n_{lm}}{\partial n_1} \frac{\partial n_1}{\partial \omega}}. \tag{5.2.5}$$

We illustrate the group velocity as a function of K at the temperature $T =$ 42nK in figure(5.14). We calculate the group velocity for the eit condition under some numerical parameters; $n_1 = 1.01968$, $2\triangle = 0.2$, $R = 21.1\mu$m and $k_0 = 1.06675 \times 10^7(1/\text{m})$. The group velocity is $v_g = 29.9$m/sec for the single mode under eit condition. As seen in the figure (5.14) group velocity increases with the mode number K which is defined as $(l + 2m + 1)$. The normalized frequency which determines the maximum mode condition is computed from definition $V = 45$. Under EIT conditions, if we compare imaginary and real parts of the susceptibility;imaginary part $\chi^{''}$ of χ is very small. We consider a gas of $N = 8.3 \times 10^6$ ^{23}Na atoms for which $M = 23$ amu, $\lambda_0 = 589$ nm, $\gamma = 2\pi \times 10.01$ MHz, $\Gamma_3 = 0.5\gamma$, $\Gamma_2 = 2\pi \times 10^3$ Hz, and $a_s = 2.75$ nm. For the parameters of

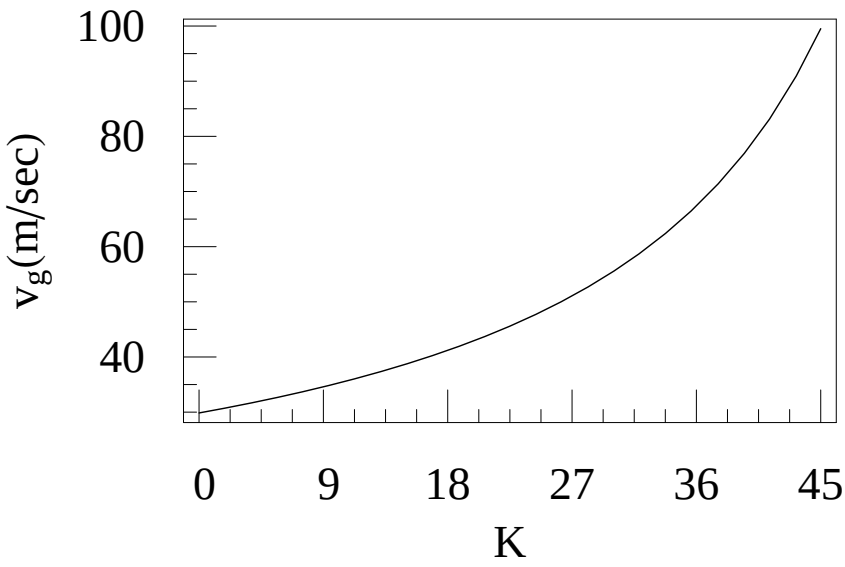


Figure 5.14: Dependence of the group velocity on $K = (l + 2m + 1)$ at $T = 42$ nK. For the single mode condition group velocity is 30.8 m/s [53, 55].

the trapping potential, we take $\omega_r = 2\pi \times 69$ Hz and $\omega_z = 2\pi \times 21$ Hz as in reference [1]. The coupling field Rabi frequency is taken to be $\Omega_c = 2.5\gamma$. For these parameters we obtain $\chi^{'} = 0.04$ and $\chi^{''} = 0.0006$. Detuning parameter is obtained for the single mode condition, $\Delta = 0.1\gamma$ where $\gamma = 6.29 \times 10^7$ 1/sec. The normalized frequency V is defined as $k_0 R_{TF}(n_0^2 - n_2^2)^{1/2}$. If we use refractive index enhancement scheme, we will get mode subscription. The parameter V determines the number of mode supported by the fiber.The refractive index is defined as $n_1 = (1 + \chi)^{1/2}$. In practice the parabolic-index profile is truncated at the core boundary $r = R_{TF}$. We find a confined mode description for the propagation constant,β, $k_0 < \beta < n_0 k_0$. The subscription is

$$2(l + 2m + 1) \leq n_1 k_0 R\sqrt{A} = V \tag{5.2.6}$$

where $V = k_0 R(n_1^2 - n_2^2)^{1/2}$, $A = 0.2$, for $r > R$ n_2 is the clad refractive index, $n_2 = n_0(1 - 2\triangle)^{1/2}$ or $n_2 = 1$. As seen in in the Figure 5.15 the lowest value of the V is 7.3 at temperature 398.7nK. The dimensionless normalized frequency V is defined as $V = n_1 k_0 R\sqrt{A} = k_0 R(n_1^2 - 1)^{1/2}$. Its thermal behavior is plotted in Figure 5.15. Multiple-mode support can be perhaps most conveniently tuned by T. For the parameters used in Figure 5.14, at $T = 42$ nK it starts from $V = 45$ and decreases down to a lowest value of $V \approx 7.3$ at $T = 398.7$ nK. As temperature increases, thermal size of the condensed cloud shrinks and the index contrast

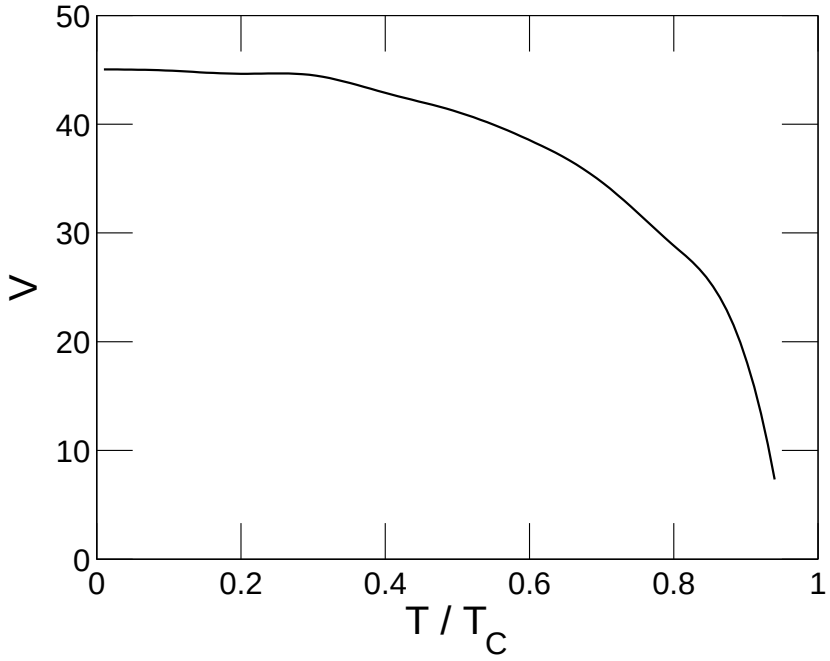


Figure 5.15: Temperature dependence of V in EIT scheme. Parameters used are $a_s = 2.75$ nm, $\lambda = 589$ nm, $N = 8.3 \times 10^6$ ^{23}Na atoms, $\omega_r = 2\pi \times 69$ Hz, $\omega_z = 2\pi \times 21$ Hz

diminish so that the BEC can no longer support multiple mode propagation. The parameter V determines the number of modes that can supported by the atomic cloud. We find a confined mode description via $k_0 < \beta < n_1 k_0$ so that $K \leq V/2$. A condensate supports only single LP_{00} mode for $2 \leq V < 4$. For $2 \leq V < 6$, it could support just two modes, LP_{00} and LP_{10}. V can be tuned by various experimental parameters as $V = k_0\mu(2\chi_1'/m\omega_r^2 u_0)^{1/2}$. [53, 55].

More accurate results may be obtained using a numerical scheme. For that purpose it is assumed that the index of refraction increases incrementally from the edge to the center of the core. If the number of increments is high enough, this model will be a faithful representation of the conditions prevailing in the inhomogeneous core. Within each increment the refractive index is constant and we can use exact solutions of the wave equation in terms of Bessel functions. Electromagnetic boundary conditions provide a recurrence relation between successive solutions as well as an equation for the propagation constant. We have compared the results of our numerical calculation with these of WKB calculations and found excellent agreement. Typical results of our numerical simulations is

given in Figure 5.16, where the modes LP_{00} and LP_{10} are shown. [53, 55]

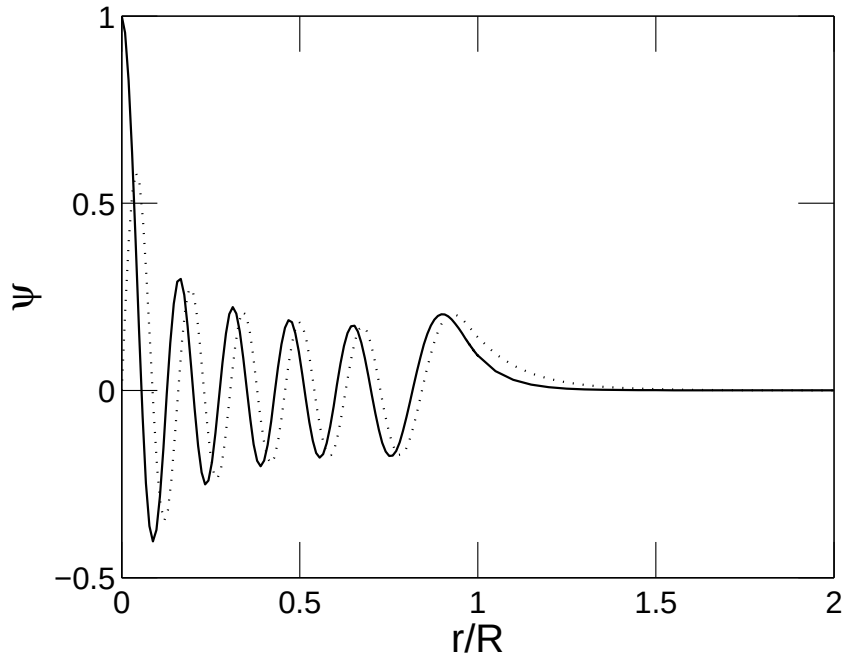


Figure 5.16: Radial profiles of transverse modes LP_{00} and LP_{10} confined in a BEC of ^{23}Na atoms with parameters given in the figure 5.15.

5.3 Optical waveguiding under refractive index enhancement scheme

We obtain many modes if we use refractive index enhancement scheme. From equation(5.2.6) we have found single mode condition. If someone wants to get many modes at low temperature, he or she can use refractive index enhancement scheme. In this scheme there is no absorption but the value of the group velocity is not slow as in the EIT scheme. Atomic coherence lead to cancellation of absorption in the refractive index enhancement scheme[49]. If we write single-mode condition($l = 0$ and $m = 0$) for the Bose-Einstein Condensate, we will obtain

$$2 \leq V < 4. \tag{5.3.7}$$

For $2 \leq V < 6$, it could support just two modes, LP_{00} and LP_{10}. When we use refractive index enhancement scheme for the condensate, we show four modes $LP_{00}, LP_{01}, LP_{02}, LP_{03}$.

We have compared the results of our numerical calculation with these of WKB calculations and found excellent agreement as seen in the table (5.1) and table

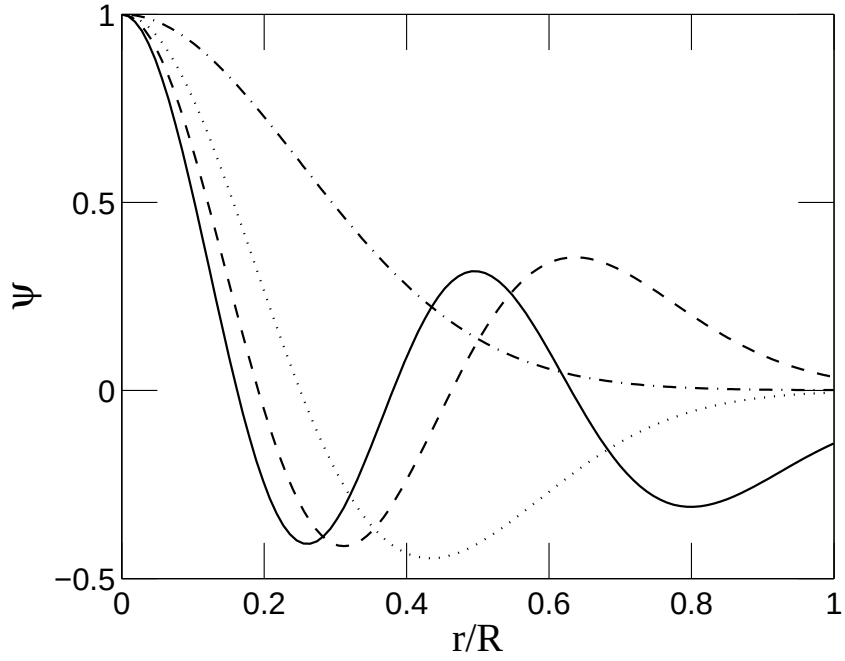


Figure 5.17: LP_{00}, LP_{01}, LP_{02}, LP_{03} are displayed. Each $\psi(r)$ is shown and the smallest root is solid line.

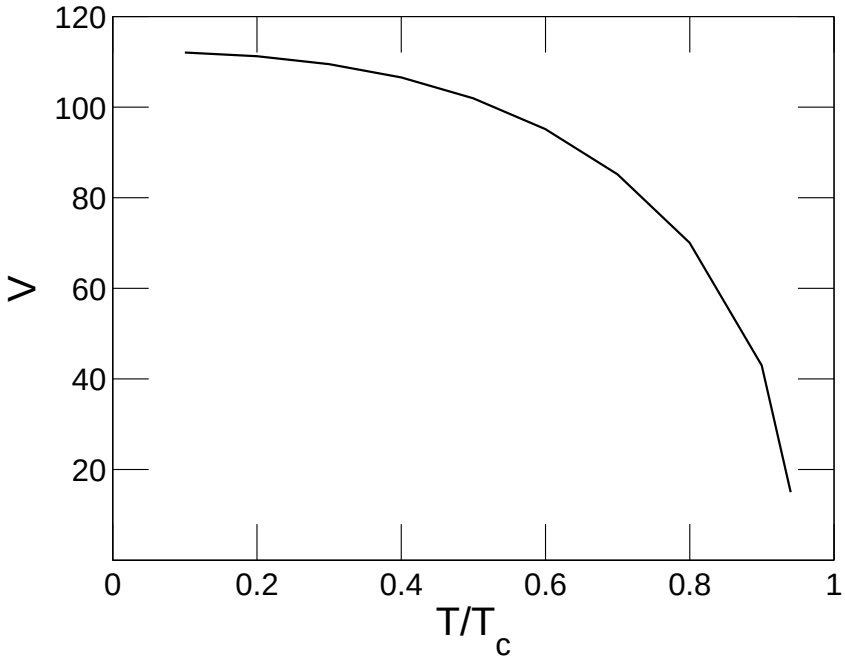


Figure 5.18: Temperature dependent of V in refractive index enhancement scheme. Parameters used are: Scattering length, $a_s = 2.75$nm, $\lambda = 589$nm, $N = 8.3 \times 10^6$, $\omega_r = 2\pi \times 69$Hz, $\omega_z = 2\pi \times 21$Hz, $M = 23$amu as for the experiment [1].

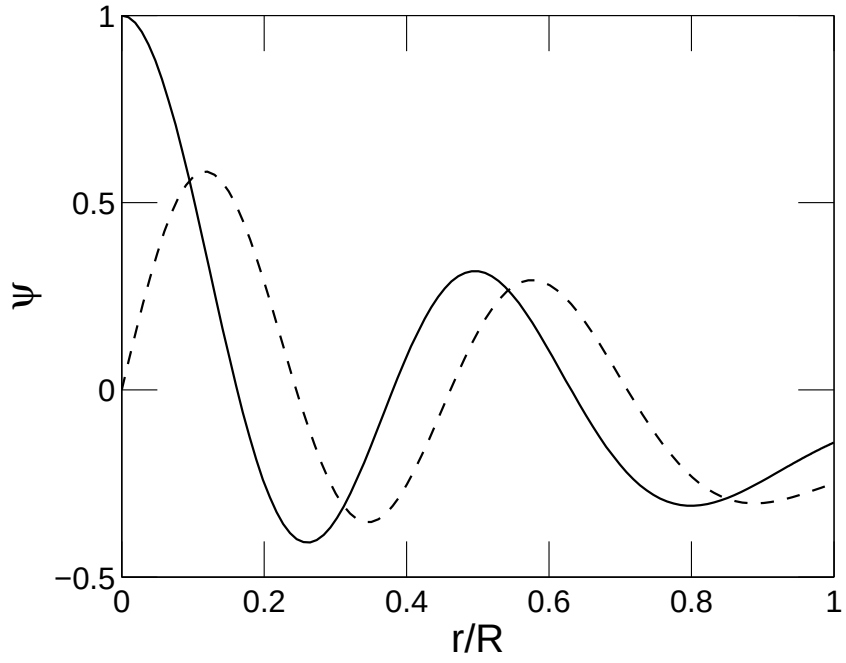


Figure 5.19: Radial profiles of transverse modes LP_{00} and LP_{10} confined in a BEC of ^{23}Na atoms with parameters given in the figure 5.18.

Table 5.1: Propagation constants obtained by WKB method

	$\beta_1 R$	$\beta_2 R$	$\beta_3 R$	$\beta_4 R$
$l = 0$	32.4740	33.4395	34.3779	35.2914
$l = 1$	31.9803	32.9603	33.9119	34.8376

(5.2). We calculate wave number, β_{lm} in the z direction. The WKB values of the propagation constant β_{lm} of the graded-index model is identical to that given by the numerical method. As seen in in the figure 5.18 the lowest value of the V is 15.01 at temperature 398.7nK. Moreover there are many modes in refractive index enhancement scheme at low temperatures.

5.4 Compensation of ultraslow short pulses by nonlinear term

In our numerical calculations of the theoretical results presented in the preceding section, we shall specifically consider a gas of $N = 8.3 \times 10^6$ ^{23}Na atoms for which

Table 5.2: Numerically evaluated propagation constants

	$\beta_1 R$	$\beta_2 R$	$\beta_3 R$	$\beta_4 R$
$l = 0$	32.4914	33.4400	34.3778	35.2912
$l = 1$	32.0661	32.9635	33.9119	34.8375

$M = 23$ amu, $\lambda_0 = 589$ nm, $\gamma = 2\pi \times 10.01$ MHz, $\Gamma_3 = 0.5\gamma$, $\Gamma_2 = 2\pi \times 10^3$ Hz, and $a_s = 2.75$ nm. For the parameters of the trapping potential, we take $\omega_r = 2\pi \times 69$ Hz and $\omega_z = 2\pi \times 21$ Hz as in reference [1]. The coupling field Rabi frequency is taken to be $\Omega_c = 5\gamma$[1]. Critical temperature for Bose-Einstein condensation for such a gas is found to be $T_C = 424$ nK. If we calculate the transmission

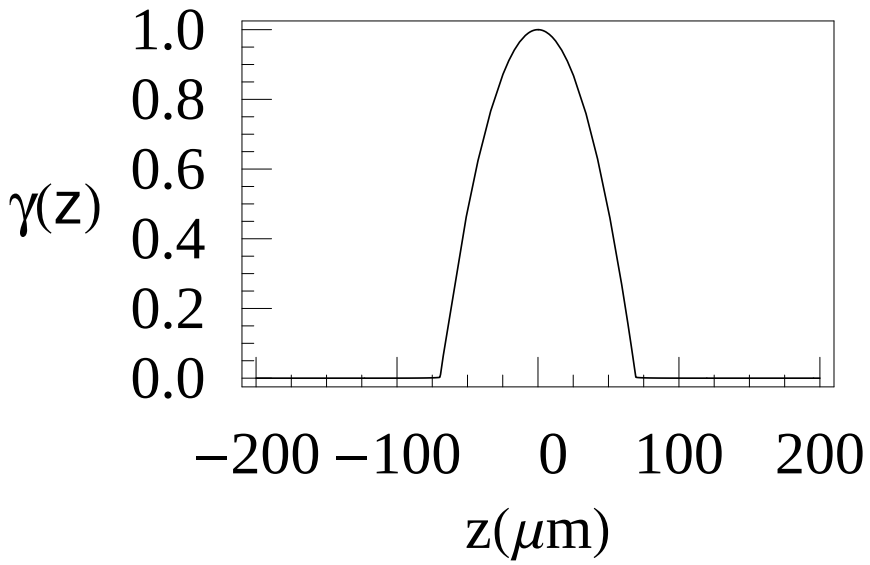


Figure 5.20: Axial spatial profile of the nonlinear coefficient γ for the parameters same with those of figure(5.4). γ is normalized by 1.437×10^{-3}

window, $\Delta\omega_{trans}$ by using the parameters which have been mentioned above, we find $\Delta\omega_{trans} = 8.49 \times 10^7$ and $\Delta T = 0.01\mu$sec. In figure(5.20) and figure(5.21) axial spatial profile of the nonlinear optical Kerr coefficient and second-order dispersion coefficient are shown. Second-order dispersion coefficient is normalized by the peak value $\beta_2(0) = 1.06 \times 10^{-11}$.

The study of pulse propagation in the mediums which includes the nonlinear effects involves short pulses with widths ranging from 10nsec to 10fsec[57]. Equation(4.6.48) can be written in the following form

$$\frac{\partial E}{\partial z} + \frac{\alpha'}{2}E + \beta_1 \frac{\partial E}{\partial t} + \frac{i}{2}\beta_2 \frac{\partial^2 E}{\partial t^2} + i\eta|E|^2 E = 0. \tag{5.4.8}$$

Here $\beta_1 = 1/v_g$, $\beta_2 = 2b_2$ and $\alpha' = 2\alpha$. Nonlinear coefficient $\eta = -(\pi/\lambda)\chi^3(\omega_0)$. By making transformation $T = t - z/v_g$, $A = \sqrt{\epsilon_0 c}E$ and $\gamma = \eta/\epsilon_0 c$ [57], we will obtain

$$i\frac{\partial A}{\partial z} + \frac{\alpha'}{2}A - \frac{1}{2}\beta_2 \frac{\partial^2 A}{\partial T^2} + \gamma|A|^2 A = 0. \tag{5.4.9}$$

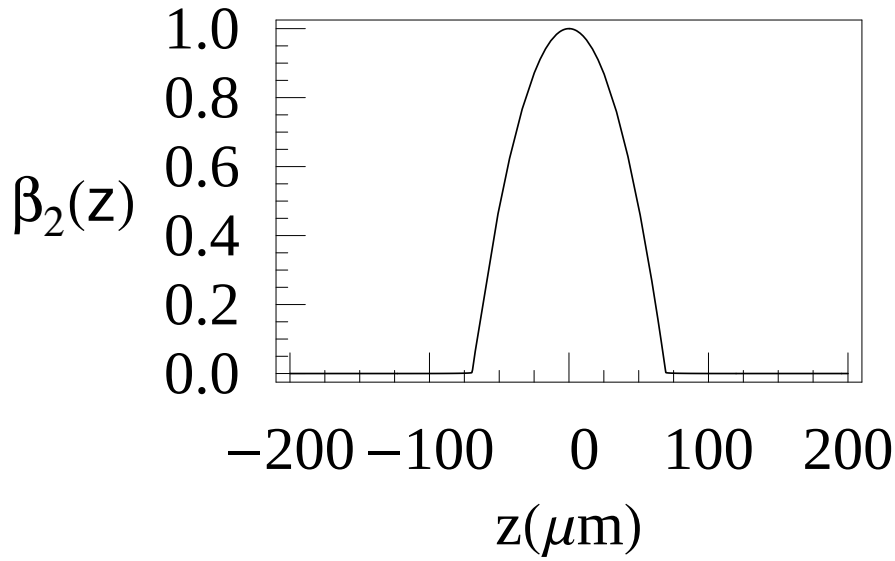


Figure 5.21: Axial spatial profile of the second-order dispersion coefficient β_2 for the parameters same with those of figure(5.4). β_2 is normalized by 1.06×10^{-11}

where A is the slowly varying amplitude of the pulse envelope. We define $\gamma = \eta/\epsilon_0 c$, and T is measured in a frame of reference moving with the pulse at the group velocity v_g.

5.5 Group-velocity dispersion and self-phase modulation

In order to solve equation(5.4.9) one can introduce normalized amplitude U by using the definition[57]

$$A(z,\tau) = \sqrt{P_0} exp(-\alpha' z/2) U(z,\tau). \tag{5.5.10}$$

where P_0 is the peak power of the incident pulse, $\tau = T/T_0$ with initial pulse T_0. The dispersion length L_D and the nonlinear length L_{NL} provide length scales over which dispersive or nonlinear effects become important for the pulse evolution in the Bose-Einstein condensate with length L. The dispersion length L_D and the nonlinear length L_{NL} are denoted as[57]

$$L_D = \frac{T_0^2}{|\beta_2|}, \tag{5.5.11}$$

$$L_{NL} = \frac{1}{\gamma P_0}. \tag{5.5.12}$$

For the nonlinear pulse propagation, the parameter N which is dimensionless is defined as

$$N^2 = \frac{L_D}{L_{NL}} = \frac{\gamma P_0 T_0^2}{|\beta_2|}. \tag{5.5.13}$$

Here $\gamma = \eta/\epsilon_0 c$, and c is the speed of light. For values $N \approx 1$ both Self-phase modulation(SPM) and Group-velocity dispersion(GVD) play an equallay role[57]. Finally we find a peak power that compensate the group-velocity dispersion for the width 0.01μsec optical pulse which is propagating in the BEC.

$$P_0 = \frac{|\beta_2|}{T_0^2 \gamma}. \tag{5.5.14}$$

We have found the peak power for the width 0.01μsec of pulse, $P_0 = 5.6 \times 10^7 W$ by using equation(5.5.14). The dispersion length and the nonlinear length are $L_D = 9.4\mu$m, $L_{NL} = 12.9\mu$m.

6 CONCLUSION

Ultra-slow light, which is achieved via EIT in BECs, has an effectively long optical path lengths within the condensates. Therefore dispersive effects, in particular temporal broadening of the pulse, can be seen within the short (micrometer) length of BEC. Normally, one would need much longer distances to be covered with the pulse propagating in other more usual medium such as an optical fiber. Though dispersion has no effect on the slowing down the pulse, slow group velocity makes the dispersion visible in such a short distance.

We examined propagation of short laser pulses in a Bose-Einstein condensate taking into account the dispersive effects under the conditions for electromagnetically induced transparency. Our calculation of the high order dispersion coefficients using typical experimental parameters of slow-light schemes show that dispersive effects start to become influential for pulses whose widths are about 10^{-7}s. Present experiments uses microsecond pulses which are below that dispersion limit.

We have examined dispersive effects on short pulse propagation through a semi-ideal BEC under EIT scheme. We have found that third and higher order dispersion coefficients are negligibly small for current experimental systems. Distortion of the shape of a short pulse in the atomic cloud would be a temporal broadening arising from second-order dispersion per se. For pulses of widths greater than microseconds we have found that second order dispersion is also negligible. For microsecond pulses the broadening is about 1.7 of the initial width. As a rule of thumb, when the pulse length is broadened by less than a factor of 2, the pulse can be considered to be not significantly distorted.

Second order dispersion of the atomic cloud depends on its density profile, which is determined mainly by temperature and atomic interactions. For nanosecond pulses, we have presented the dependence of the broadening on the temperature and interatomic scattering. The broadening is found to be making a peak just below the critical temperature T_C. As the scattering length increases, the

broadening decreases at all temperatures, resulting in a lower peak.

Furthermore, we have numerically examined the effect of spatial variations of the atomic cloud. Our results indicate that due to spatial inhomogeneity the broadening is less than that predicted by the calculations based upon effective central dispersive zone. As the pulse is already broadened relative to its original width, when it arrives at the central zone, it suffers less from the high dispersive properties of this region. Qualitatively, we have found effective central zone estimations describe the behavior of the broadening very well. Our numerical simulations showed that the transmitted pulse shape in the ultraslow light experiments starts to get distorted for pulses of widths shorter than or equal to microsecond.

Finally we have shown that despite the dispersive effects it is still possible to achieve significant increase of bit storage capacity by carefully choosing a critical coupling field Rabi frequency. Though shorter pulses allow for higher capacity for a wide range of Rabi frequencies of the coupling field, the maximum achievable capacity is independent of the initial pulse width of the probe pulse and determined by the properties of the atomic cloud only.

Our results may be used for measuring T_C and a_s of the BEC medium by comparing the group speed and the broadening of the probe pulse with a reference pulse propagating in the absence of medium. One may also exploit Feshbach resonances to tune a_s to control broadening. Further uses of our results may be found in pulse shape engineering, frequency filtering, and enhancing capacity of dynamic optical memories.

We have modelled Bose-Einstein condensate in the graded-index fiber. we have examined optical waveguiding of ultraslow pulses in a Bose-Einstein condensate under EIT conditions. Off-resonant EIT scheme has been considered to permit multi-mode ultraslow light propagation. Propagation constant is calculated analytically using WKB approximation. Group velocity is shown to be larger for higher modes. Transverse LP mode profiles are determined by detailed numerical simulations. Single and two mode conditions are established in terms of experimentally accessible parameters. Temperature dependence of the number of modes that can be supported by BEC is presented. Such ultraslow modes may be useful for realizing spatially controllable storage of coherent optical information with higher capacity in BECs. We have discussed light modes of the Bose-Einstein

condensate in the graded index fiber. We find the propagation constant β_{lm}in the z direction by WKB approximation and by numerical methods. Also we find mode subscription which is shown in the equation (5.2.6). Radiuses for the single and two mode condition are analytically calculated. Using EIT, we have examined group velocity. It depends on mode number K.

Moreover, we have numerically examined optic modes and propagation constant in the z direction in the graded-index fiber. Our results show that propagation constant β is approximately same as that predicted by the analytically calculations with WKB approximation. For optical communication purposes graded-index profile is important due to its mode dispersion properties. In order to enhance quantum information and storage, three dimensional considerations may helpful. Lastly, we have found characteristic dispersion length and effective length that characterize the influence of the nonlinearity.

REFERENCES

[1] **L.V. Hau, S.E. Harris, Z. Dutton, and C.H. Behroozi**, 1999. Light speed reduction to 17 metres per second in an ultracold atomic gas," *Nature* **397,** 594-598.

[2] **D. Budker, D. F. Kimball, S. M. Rochester, and V. V. Yashchuk**, 1999. Nonlinear Magneto-optics and Reduced Group Velocity of Light in Atomic Vapor with Slow Ground State Relaxation, *Phys. Rev. Lett.* **83,** 1767-1770.

[3] **M. M. Kash, V. A. Sautenkov, A. S. Zibrov, L. Hollberg, G. R. Welch, M. D. Lukin, Y. Rostovtsev, E. S. Fry, and M. O. Scully**, 1999. Ultraslow Group Velocity and Enhanced Nonlinear Optical Effects in a Coherently Driven Hot Atomic Gas, *Phys. Rev. Lett.* **82,** 5229-5232.

[4] **S. E. Harris**, 1997. Electromagnetically induced transparency, *Physics Today* **50,** 36-42.

[5] **J. P. Marangos**, 1998. Topical review: Electromagnetically induced transparency, *J. Mod. Opt.* **45,** 471-503.

[6] **M. D. Lukin**, 2003. Colloquium: Trapping and manipulating photon states in atomic ensembles, *Rev. Mod. Physics* **75,** 457-472.

[7] **M. Fleischhauer, A. Imamoglu, and J. P. Marangos**, 2005. Electromagnetically induced transparency: Optics in coherent media, *Rev. Mod. Physics* **77,** 633-673.

[8] **M. D. Lukin and A. Imamoglu**, 2000. Nonlinear optics and quantum entanglement of ultraslow single photons, *Phys. Rev. Lett.* **84,** 1419-1422.

[9] **H. Kang, G. Hernandez, and Y. Zhu**, 2004. Resonant four-wave mixing with slow light, *Phys. Rev. A* **70,** 061804(R).

[10] **M. Fleischhauer and M. D. Lukin**, 2000. Dark-State Polaritons in Electromagnetically Induced Transparency, *Phys. Rev. Lett.* **84,** 5094-5097.

[11] **M. D. Lukin, S. F. Yelin, and M. Fleischhauer**, 2000. Entanglement of Atomic Ensembles by Trapping Correlated Photon States, *Phys. Rev. Lett.* **84,** 4232-4235.

[12] **M. D. Lukin and A. Imamoglu**, 2001. Controlling photons using electromagnetically induced transparency, *Nature* **413,**, 273-276.

[13] **D. F. Phillips, A. Fleischhauer, A. Mair, R. L. Walsworth , and M. D. Lukin**, 2001. Storage of Light in Atomic Vapor, *Phys. Rev. Lett.* **86,** 783786.

[14] **Y. Li, P. Zhang, P. Zanardi, and C. P. Sun**, 2004. Non-Abelian geometric quantum memory with an atomic ensemble, *Phys. Rev. A* **70,** 032330.

[15] **C. Liu, Z. Dutton, C. H. Behroozi, and L. V. Hau**, 2001. Observation of coherent optical information storage in an atomic medium using halted light pulses, *Nature* **409,** 490-493.

[16] **X.-G. Wei, J.-H. Wu, G.-X. Sun, Z. Shao, Z.-H. Kang, Y. Jiang, and J.-Y. Gao**,2005. Splitting of an electromagnetically induced transparency window of rubidium atoms in a static magnetic field, *Phys. Rev. A* **72,** 023806.

[17] **V. A. Sautenkov, Y. V. Rostovtsev, C. Y. Ye, G. R. Welch, O. Kocharovskaya, and M. O. Scully**, 2005. Electromagnetically induced transparency in rubidium vapor prepared by a comb of short optical pulses, *Phys. Rev. A* **71,** 063804.

[18] **Q. Sun, Y. V. Rostovtsev, J. P. Dowling, M. O. Scully, and M. S. Zubairy**, 2005. Optically controlled delays for broadband pulses, *Phys. Rev. A* **72,** 031802(R).

[19] **M. Bashkansky, G. Beadie, Z. Dutton, F. K. Fatemi, J. Reintjes, and M. Steiner**, 2005. Slow-light dynamics of large-bandwidth pulses in warm rubidium vapor, *Phys. Rev. A* **72,** 033819.

[20] **S. E. Harris, J. E. Field, and A. Kasapi**, 1992. Dispersive properties of electromagnetically induced transparency *Phys. Rev. A* **46,** R29.

[21] **M. M. Kash, V. A. Sautenkov, A. S. Zibrov, L. Hollberg, G. R. Welch, M. D. Lukin, Y. Rostovtsev, E. S. Fry, and M. O. Scully**, 1999. Ultraslow Group Velocity and Enhanced Nonlinear Optical Effects in a Coherently Driven Hot Atomic Gas, *Phys. Rev. Lett.* **82,** 5229-5232.

[22] **D. Budker, D. F. Kimball, S. M. Rochester, and V. V. Yashchuk**, 1999. Nonlinear Magneto-optics and Reduced Group Velocity of Light in Atomic Vapor with Slow Ground State Relaxation, *Phys. Rev. Lett.* **83,** 1767-1770.

[23] **A. V. Turukhin, V. S. Sudarshanam, M. S. Shahriar, J. A. Musser, B. S. Ham, P. R. Hemmer**, 2002. Observation of Ultraslow and Stored Light Pulses in a Solid, *Phys. Rev. Lett.* **88,** 023602.

[24] **M. H. Anderson, J. R. Ensher, M. R. Matthews, C. E. Wiemann, and E. A. Cornell**, 1995. Observation of Bose-Einstein condensation in a dilute atomic vapor, *Science* **269,** 198.

[25] **K. B. Davis, M.-O. Meves. M. R. Andrews, N. J. van Druten, D. S. Durfee, D. M. Kurn, and W. Ketterle**, 1995. Bose-Einstein condensation in a gas of sodium atoms, *Phys. Rev. Lett.* **75,** 3969.

[26] **G. Morigi and G. Agarwal**, 2000. Temperature variation of ultraslow light in a cold gas, *Phys. Rev. A* **62,** 013801.

[27] **W. Zhang, Z. Xu, and L. You**, 2005. Effective Size of a Trapped Atomic Bose Gas, *Phys. Rev. A* **72,** 053627.

[28] **S. Giorgini, L. P. Pitaevskii, S. Stringari**, 1997. Thermodynamics of a Trapped Bose-Condensed Gas, *J. Low Temp. Phys.* **109,** 309-355.

[29] **M. Naraschewski, D. M. Stamper-Kurn**, 1998. Analytical description of a trapped semi-ideal Bose gas at finite temperature, *Phys. Rev. A* **58,** 2423-2426.

[30] **V.V. Goldman, I.F. Silvera, and A.J. Leggett**, 1981. Atomic hydrogen in an inhomogeneous magnetic field: Density profile and Bose-Einstein condensation, *Phys. Rev. B* **24,** 2870-2873.

[31] **G. Baym and C.J. Pethick**, 1996. Ground-State Properties of Magnetically Trapped Bose-Condensed Rubidium Gas, *Phys. Rev. Lett.* **76,** 6-9.

[32] **E.P. Gross**, 1961. Structure of Quantized Vortex, *Nuovo Cimento* **20,** 454.

[33] **L.P. Pitaevskii**, 1961. Vortex lines in an imperfect Bose gas, Zh. Eksp. Teor. Fiz. **40,** 646. [Sov. Phys. JETP **13,** 451-454 (1961)].

[34] **V. Bagnato, D.E. Pritchard, D. Kleppner**, 1987. Bose-Einstein condensation in an external potential, *Phys. Rev. A***35,** 4354-4358.

[35] **Ö. Müstecaplıoğlu and L. You**,2001. Propagation of raman-matched laser pulses through a Bose-Einstein condensate, *Opt. Commun.* **193**, 301-312.

[36] **Ö. Müstecaplıoğlu and L. You**, 2001. Slow light propagation in trapped atomic quatum gases, *Phys. Rev. A* **64** 013604

[37] **P. O. Fedichev, Yu. Kagan, G. V. Shlyapnikov, and J. T. M. Walraven**, 1996. Influence of Nearly Resonant Light on the Scattering Length in Low-Temperature Atomic Gases, *Phys. Rev. Lett.* **77,** 2913-2916.

[38] **J. L. Bohn and P. S. Juliene**, 1997. Prospects for influencing scattering lengths with far-off-resonant light, *Phys. Rev. A* **56,** 1486-1491.

[39] **S. Inouye, M. R. Andrews, J. Stenger, H.-J. Miesner, D. M. Stamper-Kurn, and W. Ketterle**, 1998. Observation of Feshbach resonances in a Bose-Einstein condensate, *Nature* (London) **392,** 151-154.

[40] **A. Dogariu, A. Kuzmich, and L. J. Wang**, 2001. Transparent anomalous dispersion and superliminal light-pulse propagation at a negative group velocity, *Phys. Rev. A* **63**, 053806.

[41] **L.J. Wang, A. Kuzmich, and A. Dogariu**, 2000. Gain-assited superluminal light propagation, *Nature* **406**, 277.

[42] **G.S. Agarwal, T.N. Dey, and S. Menon**, 2001. Knob for chancing light propagation from subluminal to superluminal, *Phys. Rev. A* **64**, 053809.

[43] **M. Artoni, G. La Rocca, F. Cataliotti, and F. Bassani**, 2001. Highly anomalous group velocity of light in ultracold rubidium gases, *Phys. Rev. A* **63**, 023805.

[44] **O. Kocharovskaya, Y. Rostovtsev, and M.O. Scully**, 2001. Stopping light via hot atoms, *Phys. Rev. Lett.* **86**, 628.

[45] **P. Arve, P. Jänes, and L. Thylén**, 2004. Propagation of two-dimensional pulses in electromagnetically induced transparency media, *Phys. Rev. A* **69**, 063809.

[46] **L.-M. Duan, J.I. Cirac, and P. Zoller**, 2002. Three-dimensional theory for interaction between atomic ensembles and free-space light, *Phys. Rev. A* **66**, 023818.

[47] **G.S. Agarwal and S. Das Gupta**, 2002. *Phys. Rev. A* **65**, 053811.

[48] **H. Gao, M. Rosenberry, and H. Batelaan**, 2003. Light storage with light of arbitrary polarization, *Phys. Rev. A* **67**, 053807.

[49] **M. Scully**, 1991. Enhancement of the index of refraction via quantum coherence, *Phys. Rev. Lett.* **67,** 1855.

[50] **D. Tarhan, S. Sefi, and Ö. Müstecaplıoğlu**, 2006. Propagation of short pulses through a Bose-Einstein condensate, *Journal of Physcis:Conference Series* **36,** 194-199.

[51] **D. Tarhan, A. Sennaroglu, and Ö. Müstecaplıoğlu**, 2006. Dispersive effects on optical information storage in Bose-Einstein condensates using ultra-slow short pulses, *Journal of Optical Society of America B* **23(9),** 1925-1933.

[52] **Ö. Müstecaplıoğlu and D. Tarhan**, 2007. Enhancing capacity of coherent optical information storage and transfer in a Bose-Einstein condensate, *Laser Physics* **17(2),** 157-161.

[53] **D. Tarhan, N. Postacioglu, and Ö. Müstecaplıoğlu**, 2007. Ultraslow optical waveguiding in an atomic Bose-Einstein condensate. *Optics Letters* **32(9),** in press.

[54] **D. Tarhan, N. Postacioglu, and Ö. Müstecaplıoğlu**, 2006. Enhanced optical information storage in Bose-Einstein condenstates, *XX International Conference on Atomic Physcis*, Poster B.93, 357, Innsbruck, Austria, (2006)

[55] **Ö. Müstecaplıoğlu and D. Tarhan**, 2007. Ultraslow optical modes in Bose-Einstein Condensates, accepted in *Photonic Materials, Devices, and Applications*, Proceedings of SPIE (SPIE, Bellingham, WA, 2007)

[56] **M. O. Scully and M. S. Zubairy**, 1997. Quantum Optics, Cambridge Press, Cambridge.

[57] **G. P. Agrawal**, 1995. Nonlinear Fiber Optics, Academic Press,San Diego, California.

[58] **A. L. Garcia**, 2000. Numerical methods for physics, Prentice Hall, New York.

[59] **A. Yariv**, 1991. Optical Electronics, (Saunders College,Holt,Rinehart and Wiston, pp.101.

[60] **C. J. Pethick, H. Smith**, 2004. Bose-Einstein Condensation in Dilute Gases, Cambridge Press, Cambridge.

[61] **B. E. A. Saleh and M. C. Teich**, 1991. Fundamentals of photonics, John Wiley and Sons, Inc., New York.

[62] **L. D. Landau and E. M. Lifshitz**, 1958. Quantum Mechanics, Pergamon Press.

BIOGRAPHY

Devrim Tarhan was born in Güney in 1977. He graduated from the Denizli Anatolian High School in 1994. He obtained his BSc. degree in 1998 from Ege University, Department of Physics. He won YLE examination and he came for the graduate education to İstanbul Technical University. He obtained MSc. degree in 2002 from İstanbul Technical University, Department of Physics . He started PhD education at the same department in 2002. He is married with Nilgün Tarhan. He has been working in İstanbul Technical University, Institute of Science and Technology as a research assistant since 1999.